Type I interferons sensitise HIV-1-reactivating T-cells for NK cell-mediated elimination despite HDACi-imposed dysregulation of innate immunity

Julia Prigann[1,2,3], Dylan Postmus[1,2], Anna Julia Pietrobon[1,2], Emanuel Wyler[4], Jenny Jansen[1,2], Lars Möller[5], Jelizaveta Fadejeva[1,2], Thijs H. Steijaert[1,2], Cornelius Fischer[6], Uwe Koppe[7], Barbara Gunsenheimer-Bartmeyer[7], Karolin Meixenberger[8], Sarah N. Vitcetz[6], Madlen Sohn[6], Lucie Loyal[9], Andreas Thiel[9], Sascha Sauer[6], Kathrin Sutter[10], Ulf Dittmer[10], Michael Laue[4], Norbert Bannert[6], Markus Landthaler[3,11] and Christine Goffinet[1,2,12]

[1]Institute of Virology, Charité - Universitätsmedizin Berlin, Corporate Member of Freie Universität Berlin and Humboldt-Universität zu Berlin, Berlin, Germany

[2]Berlin Institute of Health (BIH), Berlin, Germany

[3]Gladstone Institute of Virology, San Francisco, CA 94158, USA

[4]Berlin Institute for Medical Systems Biology, Max Delbrück Center for Molecular Medicine in the Helmholtz Association, Berlin, Germany.

[5]Centre for Biological Threats and Special Pathogens, Robert Koch Institute, Berlin, Germany

[6]Scientific Genomics Platforms, Max Delbrück Center for Molecular Medicine in the Helmholtz Association, Berlin, Germany.

[7]Department of Infectious Disease Epidemiology, Robert Koch Institute, Berlin, Germany

[8]Sexually transmitted bacterial pathogens and HIV, Robert Koch Institute, Berlin, Germany.

[9]Si-M/"Der Simulierte Mensch" a Science Framework of Technische Universität Berlin and Charité – Universitätsmedizin Berlin, Berlin, Germany.

[10]Institute for Virology, University Hospital of Essen, Essen, Germany

[11]Institute for Biology, Humboldt-Universität zu Berlin, Berlin, Germany.

[12]Department of Tropical Disease Biology, Liverpool School of Tropical Medicine, Pembroke Place, Liverpool L3 5QA, U.K.

Christine Goffinet, Liverpool School of Tropical Medicine, Pembroke Place Liverpool, L3 5QA Liverpool, UK

Phone: +44(0)151 705 3100

e-mail: christine.goffinet@lstmed.ac.uk

Keywords: HIV-1 cure, shock-and-kill, single cell RNA-sequencing, HDACi, type I interferon

ABSTRACT

Shock-and-kill is one of the most advanced, yet unrealized, concepts towards establishment of HIV-1 cure. Treatment with latency-reversing agents (LRAs), including histone deacetylase inhibitors (HDACis) exerting chromatin remodelling and gene expression reprogramming, combined with anti-retroviral therapy reactivates HIV-1 transcription *in vitro*, *ex vivo* and *in vivo*. However, HDACi treatment fails to significantly reduce the size of the viral reservoir in people living with HIV-1 (PLHIV). Here, by combining scRNA-seq and functional approaches, we characterised the HDACi treatment-imposed remodulation of CD4+ T-cells' state and its consequences for HIV-1 latency reversal and the apparent resistance of HIV-1-reactivating cells to immune-mediated elimination. Exposure of $CD4^+$ T-cells from three aviremic PLHIV with clinically applicable concentrations of Panobinostat markedly reduced the expression of genes mediating T-cell activation and IFN-driven antiviral immunity in a largely $CD4^+$ T-cell subset-nonspecific manner, with exception of an PLHIV-specific exhausted $CD4^+$ T-cell subpopulation. Altered transcriptomic profiles were accompanied by large refractoriness to peptide and IL-2/PHA stimulation, and to exogenous type I interferon, that would otherwise induce T-cell activation and expression of a plethora of antiviral genes, respectively. Type I interferon, when added to Panobinostat during HIV-1 reactivation, was unable to counteract HDACi-mediated inhibition of IFN signalling and failed to interfere with HIV-1 reactivation *per se*. However, it imposed a pre-budding block and boosted surface levels of HIV-1 Env on reactivating cells. Co-treatment with type I IFNs, most prominently IFN-β and -α14, sensitised HIV-1-reactivating cells for killing by NK cells through antibody-dependent cytotoxicity. Together, our study provides proof-of-concept of the benefit of combining a potent LRA with immunostimulatory molecules, such as type I IFNs, to reduce the resistance of HIV-1-

reactivating T-cells to immune-mediated elimination to improve current shock-and-kill strategies.

INTRODUCTION

Antiretroviral therapy (ART) effectively suppresses viremia and has improved the quality and duration of life of people living with HIV/AIDS (PLHIV), but requires livelong adherence and is not curative (1–4). HIV-1 persists as a viral reservoir in latently infected, long-lived CD4+ T-cells with an estimated 73 years of optimal ART theoretically required for reservoir eradication (5,6).

To accomplish ART-free remission, studies have focused on the reduction of the size of the latent reservoir to achieve a functional HIV-1 cure (7). The shock-and-kill cure approach is based on the administration of latency-reversing agents (LRAs) combined with ART with the intention to reverse proviral quiescence in cellular reservoirs, an event that should be followed by specific elimination of HIV-1-reactivating cells using immunological or pharmacological mechanisms (8,9). Various classes of molecules, such as histone deacetylase inhibitors (HDACis) (10–12), protein kinase C (PKC) agonists (13–15), bromodomain and extraterminal domain (BET) protein inhibitors (16), second mitochondria-derived activator of caspases (SMAC) mimetics (17), and Toll-like receptor (TLR) agonists (18,19) have been explored for their ability to reverse HIV-1 latency *ex vivo* and *in vivo.* In clinical trials individual LRAs demonstrate clear ability to reactivate HIV-1 transcription, demonstrated by increased plasma viremia during continued ART. However, the size of the viral reservoir in most studies decreased only to a minor extent, if at all (8,20) for poorly understood reasons. One potential exception is the recent study in which treatment with Venetoclax, a pro-apoptotic inhibitor of BCL-2, delayed viral rebound in a humanised mouse model of HIV-1 infection, and depleted integrated HIV-1 DNA in $CD4^+$ T-cells from PLHIV (21), suggesting that sensitising HIV-1-positive cells to apoptosis might enable reduction of the reservoir size. Overall, existing data demonstrate an urgent need for a conceptual improvement of the shock-and-kill approach.

Besides $CD8^+$ T-cell mediated mechanisms (22), NK cell-mediated antibody-dependent cellular cytotoxicity (ADCC) has been proposed to contribute to natural, ART-free control of HIV infection *in vivo*. Specifically, potent NK cells' anti-HIV activity was identified as

a discriminatory parameter in HIV-1 elite controllers as opposed to viremic progressors (23,24) and as a specific characteristic of the few participants in the RV144 HIV-1 vaccine trial who were protected from infection after immunisation (25,26). Type I IFNs increase the potency of NK cells to eliminate HIV-1-infected cells *ex vivo* (27,28). Administration of pegylated IFN-α2a or -α2b in combination with ART has resulted in sustained viral control in PLHIV and declined levels of integrated HIV-1 DNA in the context of structured ART interruptions, observations that associated with enhanced cytotoxic NK cell activity (29–35). Overall, there is a growing body of evidence pointing towards a potential benefit of incorporating type I IFNs into LRA-involving HIV-1 cure strategies, although the individual combinations of specific LRAs with type I IFN have not yet been functionally tested in regards to both HIV-1 transcriptional reactivation and cell elimination.

Here, we characterise the transcriptional and functional profiles of $CD4^+$ T-cells from PLHIV upon *ex vivo* exposure to two HDACis, Panobinostat and Vorinostat, to explore potential cell-intrinsic properties contributing to the resistance of HIV-1-reactivating cells to immune-mediated elimination *in vivo*. Using single-cell RNA sequencing we identified *ex vivo* HDACi treatment to highly impact T-cell receptor and IFN-related innate immune signalling pathways, resulting in a strong impairment of respective functions. Despite the extensive shut-down of IFN signalling by Panobinostat treatment, type I IFN treatment, while not interfering with HIV-1 reactivation *per se*, induced a block prior to viral budding. This phenotype was accompanied by accumulation of viral Env on the surface of HIV-1-reactivating cells which translated into a higher susceptibility to NK cell-mediated ADCC as compared to cells treated with HDACi alone. In conclusion, this study provides proof-of-concept for combination of potent LRAs with type I IFNs being a promising strategy to overcome the resistance of HIV-1-reactivating T-cells to NK cell-mediated elimination. We propose that the results of our study have important implications for improving current shock-and-kill strategies and will inform future HIV-1 cure therapies.

RESULTS

Panobinostat treatment modulates expression of CD4⁺ T-cell subset-specific markers

In order to understand LRA-induced cellular phenotypes and CD4⁺ T-cell subpopulation-specific susceptibilities to HDAC inhibition, we exposed purified CD4⁺ T-cells isolated from three aviremic PLHIV (**Supplementary Table 1**) to Vorinostat, Panobinostat, IL-2/PHA or left them mock-treated for 48 hours, followed by single cell RNA-sequencing. We selected Vorinostat and Panobinostat as prototypic HDACis due to their demonstrated ability to reactivate HIV-1 RNA expression *in vivo* (36,37). The applied concentrations of Vorinostat (500 nM) and Panobinostat (50 nM) approached those detected in patients´ plasma after single oral administration (11,36–38). We included IL-2/PHA treatment as a reference that we expected to result in maximal activation of T-cells.

We used previously defined marker genes to identify the following T-cell subsets (39–41): Naïve (T_N), central memory (T_{CM}), transitory memory (T_{TM}), effector memory (T_{EM}), effector memory re-expressing CD45RA (T_{EMRA}) and regulatory (T_{REG}) T-cells in the dataset of mock-, HDACi- and IL-2/PHA-treated CD4⁺ T-cells of PLHIV (**Fig. 1A**). In line with previous studies (42), the T-cell subset distribution was not significantly altered in mock-treated samples from aviremic PLHIV undergoing ART as compared to a culture from an HIV-1-negative donor (**Fig. 1B**). However, we confirmed the previously reported presence of a small subpopulation specifically identified in cells from PLHIV (42,43), characterised by a combined and significantly higher expression of the exhaustion markers *PDCD1*, *LAG3, HAVCR2, GZMB* that was clearly separated from the otherwise similar T_{EMRA} cells (**Sup. Fig. 1**). Accordingly, we referred to this subset as exhausted T-cells (T_{EX}).

Overall, Vorinostat-treated CD4⁺ T-cell cultures displayed very mild changes in subset distribution as opposed to Panobinostat-treated culture that experience a complete loss of cells expressing markers of T_{TM} (9.34% to 0%, p = 0.0008), T_{EMRA} (5.03% to 0%, p = 0.0676) and T_{REG} (4.98% to 0%, p = 0.0161) subsets and a parallel increase in the proportion of T_{CM} (23.9% to 35.57%, p = 0.0155). Relative levels of T_N (50.25% to 54.34%, p = 0.0821), T_{EX}

(0.43% to 1.11%, p = 0.778) and T_{EM} cells (6.06% to 5.18%, p = 0.2215) remained unchanged under these experimental conditions (**Fig. 1B**). The observed changes in the T-cell subset distribution induced by the individual treatments were detected in cell cultures from all three donors to a similar extent (**Sup. Fig. 2**). Although we confirmed a low, but statistical significant increase in both early and late apoptotic T-cells following Panobinostat treatment using a flow cytometry-base viability assay, the complete loss of T_{TM}, T_{EMRA} and T_{REG} RNA marker-expressing cells is unlikely to be explained by excessive, cell-type specific cell death (**Sup. Fig. 3A-B**). Observed transcriptional changes correlated with reduced expression of multiple T-cell marker on the cell surface following Panobinostat, but not Vorinostat, treatment, including CD3, CD4, CD45RA (marker for naïve T-cells), CD62L (SELL), CD45RO (marker for memory T-cells), HLA-DR (late marker for activated T-cells), CXCR4, and most pronounced, the cytokine receptor IL7R/CD127 (**Sup. Fig. 3C**). CCR5 and CD69 cell surface expression were mildly increased in the context of Panobinostat treatment, corroborating previous reports of transient CD69 expression following Panobinostat treatment from *in vivo* (44) and *ex vivo* (38) studies (**Sup. Fig. 3D**). Together, among the two HDACi treatments conducted under indicated experimental conditions, Panobinostat induced a massive rearrangement of $CD4^+$ T-cell subset marker expression, both on the transcriptional and translational level.

Panobinostat treatment induces broad transcriptional down-modulation of genes involved in T-cell signalling and a subset of genes implicated in innate immunity

Vorinostat treatment induced modest gene expression changes, with expression of 1.388 genes induced and 312 genes decreased (**Fig. 2A**). In contrast, Panobinostat treatment altered the expression of a total of 10.119 genes. Comparing the two HDACi treatments, 4.078 genes were up-regulated and 5.124 were down-regulated in Panobinostat- compared to Vorinostat-treated cells. Focussing on genes with >2-fold change in expression, cultures treated with individual HDACis displayed a substantial overlap of DEGs, suggesting that transcriptomic alterations were partially similar (**Fig. 2B**). Gene sets previously associated with

Notch signalling, synaptic vesicle trafficking and Alzheimer's disease-presenilin were enriched in Panobinostat-treated cell cultures (**Fig. 2C**). Pathways that were downregulated in the context of Panobinostat treatment were associated with T-cell activation, cytokine- and chemokine-mediated inflammation and JAK/STAT signalling (**Fig. 2C**), in line with reduced activity of multiple transcription factors in all T-cell subsets essential for mediating innate and T-cell-specific immune responses, such as IRF9, STAT1, STAT2, NFKB1 and STAT5, GATA3, RELA, respectively (**Fig. 2D**). Interestingly, activity scores of IRF3 and STAT6 were increased in T_N- and T_{CM}-cell subsets (**Fig. 2D**), suggesting partial, subset-specific activation of innate signalling cascades. Vorinostat failed to enrich or deplete specific gene sets, corroborating the minor impact of Vorinostat at the applied concentration on the overall T-cell transcriptomic profile.

Base-line expression of IFN-stimulated genes (ISGs) in untreated cells was to a certain extent subset-specific (**Fig. 2E**). For example, *LGALS3BP* and *IFI44L* displayed the highest expression in resting T_N- and T_{CM}-cell subsets, respectively, while *OASL* and *APOBEC3G* expression was highest in T_{EM}- and T_{EMRA}-cells. The observations on the individual ISG expression level were corroborated by the IFN Module Score that takes expression of multiple genes associated with IFN signalling into account. T_N-, T_{CM}- and T_{TM}-cells displayed an overall modest, T_{EM}-, T_{EMRA}- and T_{REG}-cells gradually increasing and T_{EX}-cells a relatively low IFN Module Score in mock-treated $CD4^+$ T-cells (**Fig. 2F**). Overall, Vorinostat treatment only mildly affected the ISG expression pattern and IFN Module Score (**Fig. 2E-F**). In contrast, Panobinostat-exposed $CD4^+$ T-cells displayed drastically decreased levels of the majority of ISGs, including *ISG20*, *MX1*, *IFI44L*, *IFITM1*, *XAF1*, *GBP2*, *IFI16* throughout all subsets and reduced expression of *IFI27*, *IFITM3*, *IFIT3*, *IFIT2* and *BST2* in T_N-, T_{CM}- and T_{EM}-cells, with an opposite trend in T_{EX}-cells (**Fig. 2E**). However, *IFIT1, STAT1, IFI30 and RASD2* expression was increased after Panobinostat treatment in all subsets, with *IFIT1* and *STAT1* expression found to be most pronounced in T_{EX}-cells, and *IFI30* and *RASD2* expression to be particularly induced in T_{EM}-cells (**Fig. 2E**). Interestingly, we previously reported expression of these four genes specifically to be upregulated in the context of base-line cGAS activity (45), which drives

IRF3-controlled gene expression, suggesting a partial and $CD4^+$ T-cell subset-specific activation of IRF3 following Panobinostat treatment. Nevertheless, the overall IFN Module Score taking the average expression of hundreds of ISGs into account was decreased in all Panobinostat-treated T-cell subsets, while it was largely maintained upon Vorinostat treatment (**Fig. 2F**).

We established a drastic down-regulation of genes involved in T-cell signalling and activity following Panobinostat, but not Vorinostat treatment (**Fig. 2G-H**). As expected under mock treatment conditions, expression of genes whose products regulate and mediate T-cell signalling and activation was clearly T-cell subset-specific (**Fig. 2G-H**). Panobinostat treatment induced downregulation of expression of multiple T-cell function-specific genes, including *IL4R*, *LAT*, *IL6R*, *ZAP70*, and those for which we had detected reduced protein expression on cell surface (CD62L (*SELL*), HLA-DRA, CD45RA/CD45RO (*PTPRC*), IL7R, CCR5 and CD3 (*CD3G*)). Some T-cell-specific genes were specifically upregulated in T_{EX}-cells, including *CD4*, *MAP3K1*, *CSK* and *AKT3*. In accordance with the transient nature of CD69 expression upon Panobinostat treatment (**Sup. Fig. 3D**), *CD69* mRNA expression at 48 hours equaled those of mock-treated cells. The overall trend of reduced T-cell activation-specific gene expression was reflected in a T-cell Activation Module Score of Panobinostat-treated cells that was reduced to below the average of mock- and Vorinostat-treated cells (**Fig. 2H**).

In order to test to which extent HDACi-imposed gene expression changes can be recapitulated in a more amenable HIV-1 latency cell system, we treated J1.1 T-cells, that harbour at least two replication-competent HIV-1 proviruses per cell (46,47) with Vorinostat and Panobinostat (**Sup. Fig. 4**). Here, we applied concentrations of HDACis (16 µM Vorinostat and 200 nM Panobinostat) that induced a similar degree of HIV-1 reactivation as judged by intracellular HIV-1 p24 expression (**Sup. Fig. 4A**). Both treatments resulted in a similar number of down- and upregulated genes (**Sup. Fig. 4B**) with a substantial overlap of modulated genes (**Sup. Fig. 4C**). The concentration of applied Panobinostat in J1.1 T-cells (200 nM) approached the one used in primary $CD4^+$ T-cells (50 nM) and induced partially similar gene

expression changes. Specifically, downregulated activity scores of transcription factors required for T-cell signalling (**Sup. Fig. 4D**), in line with reduced expression of genes related to T-cell activity, such as *CD3G*, *SELL*, *LAT*, *STAT5A* or *ZAP70* and a significantly reduced T-cell Activation Module Score (**Sup. Fig. 4E**). The ISG expression profile following Panobinostat was less well conserved between J1.1 T-cells and CD4+ T-cells. While Panobinostat-treated primary $CD4^+$ and J1.1 T-cells shared expression profiles of some ISGs (downregulation of *MX1*, *MX*2, *OAS1*, *XAF1*, *BST2*; upregulation of *GBP5*, *STAT1*, *IFIT1*), they differed regarding expression of *LGALS3BP*, *GBP2*, *IFI44L*, *OASL* (**Sup. Fig. 4F**), resulting in an overall elevated IFN Module Score in J1.1 T-cells as opposed to primary $CD4^+$ T-cells.

Conclusively, under these experimental conditions, Panobinostat, and, if applied at higher concentration, also Vorinostat, significantly reduced expression of several genes that are essential for T-cell-specific immune responses and a part of IFN-modulated genes.

HDAC inhibition imposes a block to $CD4^+$ T-cell activation and type I IFN signalling

We hypothesised that HDACi-induced modulation of gene expression is of functional relevance for HIV-1 reactivation and immune recognition of reactivating cells. To investigate the result of HDACi treatment on T-cell activation, we pre-incubated $CD4^+$ T-cells from HIV-1-negative donors with HDACis prior to inducing T-cell activation by IL-2/PHA (**Fig. 3A**). Pre-incubation with DMSO or Vorinostat resulted in marked IL-2/PHA-triggered enhancement of the percentage of cells expressing the activation markers CD69, CD25, HLA-DR and also the exhaustion markers TIM-3 and PD-1, indicating successful T-cell activation. Conversely, Panobinostat pretreatment resulted in impaired induction of CD69 expression (0.49-fold changed), and in a complete lack of IL-2/PHA-mediated induction of expression of CD25, HLA-DR, TIM-3 and PD-1 (**Fig. 3A**). To study TCR-induced T-cell activation, we preincubated $CD4^+$ T-cells with HDACi followed by treatment with a universal peptide pool in combination with an anti-CD28 antibody. Expression of the early activation marker CD69 after TCR stimulation was slightly, but statistically significantly induced in Vorinostat- (1.65-fold) and to a higher extent in

Panobinostat-pretreated samples (5.5-fold), suggesting efficient initiation of T-cell activation in the presence of both HDACis (**Fig. 3B**). Expression of the middle activation marker CD25, the exhaustion marker PD-1 and the late activation marker HLA-DRA increased upon TCR stimulation in the context of Vorinostat pretreatment (2.07-, 2.07- and 1.39-fold change, respectively), suggesting that weak HDAC inhibition does not prevent TCR-specific T-cell activation. However, expression of CD25 and HLA-DRA was severely reduced in Panobinostat-pretreated cultures (0.05- and 0.47-fold change, respectively), suggestive of abortive peptide-induced T-cell activation.

We next examined the impact of HDAC inhibition on type I IFN signalling and ISG expression. Specifically, we treated $CD4^+$ T-cells isolated from HIV-1-negative donors with DMSO, Vorinostat or Panobinostat in combination with increasing concentrations of IFN-α2a and assessed cell surface expression changes of BST-2 and changes of *IFIT1* and *MX2* gene expression (**Fig. 3C-D**). We applied an increased concentration of Vorinostat in these experiments to adjust for the inferior potency of Vorinostat compared to Panobinostat that has been reported in previous studies (38,48). Both Vorinostat and Panobinostat significantly dampened base-line BST-2 cell surface expression levels, and both tested concentrations (100 and 1000 IU/ml) of IFN-α2a failed to rescue the HDACi-imposed block to BST2 surface expression (**Fig. 3C**). Interestingly, mRNA expression levels of the two ISGs *IFIT1* and *MX2* showed a divergent phenotype. Individual treatment with Vorinostat and Panobinostat, as well as addition of IFN-α2a, induced and further amplified *IFIT1* mRNA expression, respectively (**Fig. 3D**). In contrast, *MX2* mRNA expression decreased in the context of HDACi treatment, both in the absence and presence of 1000 IU/ml IFN-α2a (**Fig. 3E**). These results were paralleled in latently HIV-1-infected J1.1 T-cells in which HDAC inhibition, but not treatment with the non-HDACi LRA Bryostatin, reverted prior IFN-α2a-induced expression of MX2 in a dose-dependent manner and abolished the negative impact of IFN on early HIV-1 reactivation as judged by intracellular p24 expression (**Sup. Fig. 5A).** Co-administration of increasing doses of IFN-α2a up to 10,000 IU/ml was insufficient to counteract the HDACi-suppressed MX2 expression and did not limit the efficiency of HIV-1 reactivation, in contrast in the context

of Bryostatin treatment, IFN treatment induced MX2 expression efficiently and inhibited HIV-1 reactivation in a dose-dependent fashion (**Sup. Fig. 5B**).

Together, HDAC inhibition renders $CD4^+$ T-cells largely refractory, and/or less sensitive, to mitogen and TCR stimulation and dampens the base-line and IFN-induced expression of multiple ISGs, including the two prototypic ISGs BST-2 and MX2, while IRF3-driven expression of a small subset of ISGs remains intact and is even exacerbated. We hypothesise that the HDACi-induced cellular phenotypes both at the level of $CD4^+$ T-cells as HIV-1 reactivating target cells, and $CD4^+$ T-cell effector functions is likely to contribute to the lack of HIV-1-positive T-cell elimination *in vivo* both at the level of $CD4^+$ T-cells as HIV-1 reactivating target cells, and $CD4^+$ T-cell effector functions.

Addition of IFN-α2a to Panobinostat results in a tetherin-independent pre-budding defect

The previous data highlighted that HDAC inhibition significantly diminishes IFN-induced signalling, potentially nullifying the negative effect of IFN on HIV-1 replication. To test in detail the impact of IFN on HIV-1 reactivation and multi-round spread upon LRA treatment, J.1. T-cells were primed with a single dose of 50 nM Panobinostat in the presence or absence of IFN-α2a. The percentage of HIV-1 p24 capsid-expressing cells was initially similar, but differed starting from day three on (**Fig. 4A**, **Sup. Fig. 6**). Addition of IFN to Panobinostat reduced the abundance of p24 capsid (**Fig. 4B**) and infectivity (**Fig. 4C**) released into cell culture supernatant, effects detectable from day two and one post-treatment start on, respectively. Two days post HIV-1 reactivation, a time point at which cell-associated p24 capsid expression is statistically indistinguishable (**Fig. 4A**), the morphology of budding sites was similar and intact in both conditions (**Fig. 4D**), however, the incidence of detectable budding events per cell was reduced 2.2-fold in the context of the co-treatment (**Fig. 4E**). Importantly, this observation was obtained in the absence of tetherin-imposed attachment of virions to the cell surface or to each other (**Fig. 4D)**. This tetherin-atypical microscopic appearance, and the lack of IFN-induced tetherin upregulation when Panobinostat is present (**Fig. 4F, G**) strongly

argues against tetherin driving this antiviral phenotype, and rather suggests a defect prior to release or a tetherin-independent release defect.

IFN-induced virus pre-budding block is accompanied by accumulation of HIV-1 Env on cellular and viral membranes

Next, we assessed the nature of the IFN-imposed block prior to HIV-1 budding. Despite increasing concentrations of IFN-α2a, Panobinostat-induced cell-associated HIV-1 p24 capsid expression remained intact (**Fig. 5A**). In contrast, the p24 capsid signal intensity in corresponding supernatants (**Fig. 5B**) and normalised release (**Fig. 5C**) dose-dependently decreased in cultures co-treated with IFN-α2a. Interestingly, combined Panobinostat/IFN-α2a treatment resulted in a higher ratio of gp120 per p24 (**Fig. 5D**), suggesting a higher rate of Env incorporation in released virions in the absence of evidence for an Env processing alteration in corresponding cell lysates (**Sup. Fig. 7A**). Panobinostat, alone or in combination with IFN-α2a, increased the percentage of cells expressing HIV-1 Env on their surface (**Fig. 5E**), in line with increase of cell-associated p24 expression by both conditions (**Fig. 5A**). However, IFN-α2a addition to Panobinostat had a 1.32-fold, statistically significant increase of the mean fluorescence intensity (MFI) of Env signal on Env-positive cells as a consequence, indicating accumulation of HIV-1 Env molecules on the cell surface (**Fig. 2F**). Treatment with the JAK/STAT inhibitor Ruxolitinib preserved the increase of percentage of Env-positive cells (**Sup. Fig. 7B**), but nullified IFN-induced Env accumulation per cell (**Sup. Fig. 7C**), consistent with upregulation of Env requiring functional IFN signalling. Conclusively, combined treatment of Panobinostat and IFN-α2a results in increased quantities of HIV-1 Env on reactivating T-cells´ surfaces and released virions.

Addition of IFN-α2a to Panobinostat enhances the susceptibility of reactivating T-cells to NK-mediated antibody-dependent cellular cytotoxicity

Being the sole viral antigen presented on the virus-producing cell surface, HIV-1 Env protein serves as the major target of antibody-mediated responses. We therefore examined whether

the increased surface expression of HIV-1 Env in the context of IFN-α2a treatment renders cells more susceptible to ADCC. Specifically, we co-cultured HIV-1-reactivating, cell tracker™ Green-CMFDA-stained J1.1 T-cells and freshly isolated PBMCs in the presence of serum from PLHIV, and loss of HIV-1 p24 capsid-positive cells was monitored (**Sup. Fig. 8A**). ADCC decreased with increasing dilutions of the anti HIV-1-Env antibody-containing serum, independent of the reactivation regimen applied (**Fig. 6A-C**). Interestingly, Panobinostat treatment failed to significantly enhance ADCC as compared to DMSO treatment, suggesting that it increases the quantities of HIV-1 p24- and Env-positive cells, but not their relative susceptibility to antibody-mediated elimination. In contrast, J1.1 T-cells reactivated in the presence of IFN-α2a scored overall higher ADCC values. T-cells co-cultured with isolated NK cells, but not monocytes, displayed a statistically significant increase of ADCC in the context of IFN-α2a co-treatment as compared to Panobinostat only-treatment (**Sup. Fig. 9A, B**), arguing for a predominant role of NK cells rather than monocytes in mediating T-cell killing. In line with this, CD107a surface exposure and CD16 downregulation, which strongly correlates with NK cell activation, cytokine production and target cell lysis (47–49), were highly induced in the NK cell population of PBMCs co-cultured with J1.1 T-cells (**Sup. Fig. 9C-E**). Co-treatment of J1.1 T-cells with Panobinostat and IFN-α2a, however, did not result in notable differences of the two Panobinostat-treated conditions in regards to NK cell effector activation despite increased target cell killing in the co-culture (**Sup. Fig. 9D-E**), arguing for IFN-a2 increasing the sensitivity of target cells to killing rather than modulating effector cell activity.

We next investigated whether IFN-α2a addition modulates the kinetics of NK cell-effected ADCC against Panobinostat-treated J1.1 T-cells using live-cell imaging. Specifically, J1.1 T-cells were treated either with Panobinostat only or Panobinostat in combination with IFN-α2a for 48 hours, followed by differential staining of these two J1.1 T-cell cultures using Cell Tracker™ Green CMFDA and Cell Tracker™ Deep Red, respectively. Cells were then co-cultured with freshly isolated, unstained NK cells at a 1:1:1 ratio in the presence of serum from PLHIV and a cell death marker (blue) and imaged every three minutes for a total of four hours (**Sup. Movie 1**). The starting frame contained similar numbers of both J1.1 T-cell cultures (47

green cells, 51 red cells). As expected, the overall number of cell death marker-positive J1.1 T-cells increased over time, indicating ADCC. We did not detect profound differences regarding the duration of individual NK cell/J1.1 T-cell interactions depending on the T-cell line pretreatment (**Sup. Movie 1**). However, the percentage of cells dying until the end of the experiment, as judged by acquisition of the blue fluorescence and visual disappearance was clearly increased for cells receiving Panobinostat/IFN-α2a co-treatment (31.4%) as compared to cells pre-treated with Panobinostat alone (12.8%) (**Fig. 6E**). The number of Panobinostat/IFN-α2a-treated J1.1 T-cells showing signs of cell death increased rapidly and plateaued at 69 minutes after the start of the imaging (**Fig. 6F**). In contrast, the number of Panobinostat-treated J1.1 T-cells with signs of cell death increased only moderately and plateaued after 75 minutes (**Fig. 6F**). Despite the high mobility and intact shape of the NK cells, no more J1.1 T-cells were eliminated 75 minutes after start of the co-culture, suggesting that the remaining J1.1 T-cells either did not reactivate HIV-1 expression or were otherwise resistant to killing. Of note, a substantial fraction of NK cells that otherwise presented an intact cell shape and high mobility acquired the blue death marker over time (**Sup. Movie 1**). We hypothesise that the processes of degranulation and re-internalization of granules in highly active NK cells allow the uptake of the cell death dye from the medium, not necessarily reflecting cell death. This is in line with the observation that specifically the highly mobile, J1.1 T-cell-interacting NK cells stained positive for the cell death marker, the same population of cells that is thought to have a high cytotoxic potential.

Overall, our observations are in line with a scenario in which addition of IFN-α2a to a Panobinostat-mediated HIV-1 reactivation regimen renders HIV-1-positive cells more prone to NK cell-mediated ADCC, in line with higher levels of the major antibody target Env on the cells' surface, despite similar levels of HIV-1 reactivation.

IFN-α2a-enhanced HIV-1 Env cell surface accumulation and ADCC sensitization occur in the context of HDACi-, but not PKC agonist-mediated HIV-1 reactivation

We next tested whether IFN-α2a-mediated upregulation of HIV-1 Env and sensitivity of cells to immunological elimination occurs in conjunction with a specific class of LRA or, on the contrary, universally upon HIV-1 latency reversal. Like Panobinostat treatment, individual treatment of cells with the HDACis Vorinostat and Romidepsin, and the PKC agonist Bryostatin strongly increased the percentage of HIV-1 p24 capsid-positive cells, while the BET inhibitor JQ1 was inferior in reversing proviral quiescence (**Sup. Fig. 10A**). Overall, the percentages of HIV-1 Env-positive cells induced by Vorinostat, Romidepsin and JQ1 treatment followed the percentages of p24-positive cells. Surprisingly Bryostatin treatment, both in the absence or presence of IFN-α2a, failed to increase the percentage of Env-positive cells, despite clear HIV-1 reactivation at the level of p24 capsid (**Sup Fig. 10B**), and accordingly, both treatments did not alter susceptibility to ADCC which, surprisingly, was clearly detectable despite low surface Env levels (**Sup. Fig. 10C**). In summary, our findings suggests that IFN-α2a co-treatment enhances Env cell surface expression in the context of HDACi and the iBET JQ1, but not Bryostatin, pointing towards LRA class-specific differences in HIV-1 Env cell surface targeting and/or regulation.

The ability to restrict HIV-1 budding and facilitate elimination of HIV-1-positive T-cells is type I IFN protein-specific

Although previous HIV-1 cure strategies focused on incorporation of IFN-α2a or -α2b in shock-and-kill approaches, *in vitro* work clearly demonstrates that other members of the type I IFN family, including IFN-α6, IFN-α14 and IFN-β, display superior anti-HIV-1 properties (49–52). To investigate the breadth of type I IFN proteins to enhance susceptibility of HIV-1-reactivating cells to elimination, we selected IFN-α6, IFN-α14 and IFN-β due to their previously reported high anti-HIV-1 activity (49,50,52), IFN-α16 for its comparatively weaker activity (49,50,52) and IFN-α2 as a reference. IFN-α14 and -β treatment resulted in strongest ISG induction, as judged by quantification of *IFIT1* mRNA and BST-2 protein expression (**Sup. Fig. 11**). Upon co-treatment with Panobinostat, all tested type I IFNs, particularly IFN-α14 and -β, significantly decreased secreted infectivity (**Fig. 7A**). Surprisingly, all IFNs shared the ability to increase

435 the HIV-1 Env surface MFI (**Fig. 7B**), but differed in their ability to sensitise T-cells for
436 elimination, with IFN-α14 and -β treatment resulting in highest ADCC rates (**Fig. 7C**). It is
437 worth mentioning that the activity of the in-house generated IFN subtypes used in Fig. 7 was
438 determined using an ISRE-reporter cell line in contrast to commercial IFN-α2a (Roferon, used
439 in the rest of the study) whose activity is quantified in a cytopathic effect inhibition assay.
440 These differences hindered a direct comparison of the two IFN-α2 potencies and potentially
441 explain the relative lack of IFN-α2 in inducing ADCC under these experimental conditions (**Fig.**
442 **7C**). The antiviral activity of individual type I IFN proteins correlated with the induced
443 susceptibility to ADCC. The degree of upregulation of cell surface Env levels did not predict
444 ADCC susceptibility (**Fig. 7D**), suggesting that IFN-mediated enhancement of surface Env
445 levels is required, but not sufficient for sensitising cells to elimination.

446 In summary, we identified a superior ability of the clinically yet underexplored members
447 of the type I IFN family, IFN-α14 and -β, to enhance susceptibility to elimination of HIV-1-
448 reactivating T-cells which correlates with their ability to inhibit HIV-1 budding in the context of
449 Panobinostat reactivation and to accumulate viral Env on the HIV-1-reactivating cells' surface.
450

451 **DISCUSSION**

452 The overarching aim of LRA treatment in the context of HIV-1 cure is reinitiation of HIV-1
453 mRNA and protein expression to a degree that is sufficient to render a maximum of HIV-1-
454 reactivating cells immunologically visible, making them susceptible to elimination. The ability
455 of HDACis to reverse HIV-1 latency *in vitro* and *in vivo* (12,36–38,53) involves hyperacetylation
456 of histones, which leads to opening of cellular chromatin and subsequently modulation of
457 gene expression, including transcriptional reactivation from dormant HIV-1 genomes (54,55).
458 LRA treatment *per se* influences the expression profile of a plethora of cellular genes, with to
459 date poorly defined consequences on cellular processes affecting HIV-1 RNA stability, HIV-1
460 protein expression, trafficking and cell surface presentation, and finally susceptibility of HIV-
461 1-reactivating cells to cytotoxicity. An optimal shock-and-kill regimen should, on the one hand,
462 mount a proviral milieu that facilitates post-integration steps of the virus replication cycle. On

463 the other hand, in a second step, an ideal shock-and-kill regimen must render reactivating T-
464 cells susceptible to recognition and killing by $CD8^+$ T-cell and NK cell-mediated cytotoxicity,
465 processes that are orchestrated in the effector cell, among others, by functional type I IFN
466 signalling (27,56). Treatment of $CD4^+$ T-cells with Panobinostat resulted in a markedly
467 impaired ability to respond to activation stimuli, including TCR/CD28 and IL-2/PHA, in line with
468 reports of HDACi treatment-induced antigen-specific anergy of mouse lymphocytes (57).
469 Given that Panobinostat treatment compromises functionality of NK cells (58) and $CD8^+$ T-
470 cells (59,60), it is tempting to speculate that it also affects the efficiency of peptide processing
471 and presentation in HIV-1-reactivating $CD4^+$ T-cells by MHC-I molecules. Along this line,
472 HDACi treatment has been proposed to reduce cytosolic peptidase activities in *ex vivo*-HIV-
473 1-infected $CD4^+$ T-cells, resulting in modulated antigen presentation to $CD8^+$ T-cells (61).
474 Together, we suspect that these effects compromise the overall effector functions of several
475 immune cell types that would otherwise contribute to elimination of HIV-1-reactivating T-cells.
476 A second striking consequence of Panobinostat was a largely $CD4^+$ T-cell subset
477 unspecific, broad, though not entire shut-down of components of IFN-related signalling
478 pathways and functions, which is consistent with the known requirement of functional histone
479 deacetylation for IFN signalling, but not for IRF3-mediated gene expression programmes (62).
480 This leads us to propose to re-consider the contribution of several antiviral genes when
481 analysed in the context of HDACi-induced reactivation, since expression of several ISGs is
482 repressed by HDACi treatment even in the presence of high concentrations of type I IFN. A
483 striking example is our observation of an IFN-induced release defect. Iin the context of
484 Panobinostat treatment, tetherin expression is downregulated in most $CD4^+$ T-cell
485 subpopulations except the exhausted CD4+ T-cell subset, fully prevented even when type I
486 IFN is exogenously added, and the microscopic appearance of stalled budding events
487 resembles more those described in the context of ESCRT component defects (63). Together,
488 these data argue rather for a to date unknown ISG product whose IFN dependency is still
489 preserved despite HDAC inhibition.

Type I IFN treatment in conjunction with Panobinostat-mediated HIV-1 reactivation was followed by increase of HIV-1 Env molecule density on viral and HIV-1-reactivating T-cells' surfaces. HIV-1 tightly regulates the presentation of Env on the cell surface to minimise the vulnerability against humoral responses while maintaining infectivity (64). The observed Env cell surface accumulation may be an indirect consequence of the pre-budding defect, where fewer virions are detached from the producer cell, resulting in excess HIV-1 Env at the plasma membrane, and/or may be a direct consequence of the HDACi/IFN treatment combination on HIV-1 Env trafficking and recycling. The rate of internalisation of Env molecules and their conformation presented at the cell surface have been reported as determinants of the HIV-1-infected cell's susceptibility to ADCC (65–67). Our data points towards a scenario in which, in the context of Panobinostat treatment, increased Env expression on reactivating T-cells, likely with contribution of a potential ISG product, sensitises HIV-1-reactivating T-cells for NK cell-mediated elimination. This would represent a novel mechanism by which type I IFN sensitises, rather than protects, target cells for elimination. On the contrary, several studies reported type I IFNs to protect T-cells from NK cell-mediated cytotoxicity by processes involving upregulation of expression of selected inhibitory NK-cell-receptor ligands (68) and reduction of expression of natural cytotoxicity triggering receptor 1 (NCR1) ligands as evasion mechanism (69). However, these studies were not conducted in the context of pharmacological reactivation of HIV-1. Specifically, a higher proportion of Panobinostat-only treated cells remained viable at the end of the co-culture as compared to IFN-co-treated cells, indicating an intrinsic resistance to ADCC-mediated killing that was partially overcome by the addition of IFN. Importantly, we did not observe differences in the degranulation activity or cellular activation of NK cells retrieved from co-cultures with either Panobinostat- or Panobinostat/IFN-treated J1.1 cells, suggesting that the impact of IFN on NK cell effector activity is neglectable under these experimental conditions. To date, only tetherin has been identified as an IFN-stimulated factor that augments ADCC responses against HIV-1-infected cells (67,70) however, it is an unlikely candidate in the context of Panobinostat treatment due to its virtually absent expression in the context of HDAC inhibition. Adding

another layer of complexity, susceptibility to immune-mediated clearance is not determined be mere quantities of surface-accessible Env, as evidenced by our data showing clear antibody-dependent killing despite low cell surface levels of Env on target T-cells following Bryostatin-mediated latency reversal, and IFN-protein-specific ADCC susceptibilities despite similar Env cell surface levels following Panobinostat treatment. The characterisation of cellular and viral factors that determine the susceptibility of HIV-1-reactivating cells to ADCC and how these factors are manipulated by individual pharmacologic latency reversal strategies are key questions to be addressed in future studies.

In the context of HIV-1 shock-and-kill cure approaches, HDACis belong to the most thoroughly studied class of LRAs and are well tolerated *in vivo* (71,72), though administration of HDACis appears to inhibit essential immune effector functions of $CD8^+$ T-cells (60), NK cells (58,73) and reduce susceptibility of target T-cells to cytotoxic elimination as shown in our study. However, the overall high potency of HDACis to reactivate HIV-1 and the lack of alternative LRAs with better *in vivo* performance encourages the continued use of HDACis in newly launched clinical trials, especially in combination with immunomodulatory drugs to counterbalance the HDACi-mediated negative effects. Currently, HDACis are being tested in combination with pegylated IFN-α2a (Clinical trial NCT02471430), broadly neutralising antibodies (Clinical trial NCT02850016) (74,75) and therapeutic vaccine candidates (Clinical trials NCT02092116 and NCT02616874) (76). Within this conceptually broad field, our study is the first proof-of-concept that provides a mechanistic rationale that justifies incorporating type I IFNs in shock-and-kill settings to enhance the susceptibility of HIV-1-reactivating T-cells to immune-mediated elimination. Importantly, the superior ability of the clinically underexplored IFN-α14 and IFN-β over IFN-α2a to sensitise T-cells for elimination justifies their advancement for clinical trials. In conclusion, combining potent LRAs with immunomodulatory molecules, such as type I IFNs, presents a promising strategy to overcome the intrinsic and/or virus-mediated resistance of HIV-1-reactivating T-cells to NK cell-mediated killing which would be an instrumental step towards effective shock-and-kill cure strategies.

MATERIAL AND METHODS

Cell lines and primary cells

HEK293T and Tzm-bl cells were obtained from ATCC and the NIH AIDS Reagents Program and maintained in Dulbecco's modified Eagle's medium (DMEM) supplemented with 10% heat-inactivated fetal calf serum (FCS), 100 IU/ml Penicillin/Streptomycin and 2 mM L-Glutamine in a 5% CO_2 atmosphere at 37°C. Jurkat and J1.1 T-cells were obtained from the NIH AIDS Reagents Program and cultivated in RPMI 1640 supplemented with 10% heat-inactivated FCS, 100 IU/ml Penicillin/Streptomycin, 2 mM L-Glutamine, 1x MEM non-essential amino acids and 1 mM sodium pyruvate in a 5% CO_2 atmosphere at 37 °C.

Withdrawal of blood samples from healthy human donors and cell isolation were conducted with approval of the local ethics committee (Ethical review committee of Charité Berlin, vote EA4/167/19). Withdrawal of blood samples from aviremic PLHIV and cell isolation were conducted with approval of the local ethics committee (Ethical review committee of Charité Berlin, votes EA2/105/05 and EA2/024/21) in the context of the HIV-1 Seroconverter Study of the Robert-Koch-Institute (77). Available clinical information is indicated in Supplementary Table 1. Human PBMCs, $CD4^+$ T-cells, NK cells and monocytes were isolated from EDTA-anticoagulated blood by Ficoll-Hypaque centrifugation or using the EasySep Direct Human $CD4^+$ T-cell, Human NK cell or Human Monocyte $CD14^+$ Isolation kits (STEMCELL Technologies), respectively. Primary cells were cultured at 10^6 cells/ml in RPMI 1640 containing 10% heat-inactivated FCS, 100 IU/ml penicillin/streptomycin, 2 mM L-Glutamine, 1% MEM non-essential amino acids and 1 mM sodium pyruvate.

Reagents and inhibitors

The following commercial reagents were used throughout this study: Bryostatin I (Sigma Aldrich), CEFX Ultra SuperStim Pool (#PM-CEFX-1, JPT), IFN-α2a (Roche), IFN-β (Roche),

IL-2 (Merck), JQ-1 (Sigma Aldrich), Panobinostat (Cayman Chemical), PHA (Thermo Scientific), Romidepsin (Selleckchem), Ruxolitinib (STEMCELL Technologies) Vorinostat/SAHA (Abcam). Efavirenz was obtained from the NIH AIDS Reagent Program. Recombinant IFN-α subtypes 2, 6, 14 and 16 were expressed in *Escherichia coli*, purified by anion-exchange and size exclusion chromatography and tested for absence of endotoxins (50). IFN units were determined using a human retinal pigment epithelial reporter cell line stably expressing a plasmid containing the IFN-stimulated response element driving a luciferase reporter gene.

Treatment of CD4$^+$ T-cells for single cell RNA-sequencing

CD4$^+$ T-cells were mock-treated (0.05% DMSO) or treated with Vorinostat (500 nM), Panobinostat (50 nM) or IL-2 (20 IU/ml) and PHA (1 µg/ml) for 48 hours before subjecting them to the single cell RNA-sequencing pipeline. J1.1 T-cells were treated with 1.6% DMSO (DMSO I), 16000 nM Vorinostat, 0.2% DMSO (DMSO II) or 200 nM Panobinostat for 40 hours before subjecting them to single cell RNA-sequencing.

Single cell RNA-sequencing

Single cell RNA-Seq libraries were prepared with the 10x Genomics platform using the Chromium Next GEM Single Cell 3' Reagent Kits v.3.1 following manufacturer's instructions. Quality control of the libraries were performed with the KAPA Library Quantification Kit and Agilent TapeStation. Libraries were sequenced on a HiSeq4000 using the following sequencing mode: read 1: 28 bp, read 2: 91-100 bp, Index i7: 8 bp. The libraries were sequenced to reach ~20 000 reads per cell.

Single cell RNA-sequencing data analysis

FASTQ files from the sequencing protocol were processed using the Cell Ranger pipeline v 3.1.0 (10X Genomics) and further analysed using the Seurat v3.1.4 package (78) in R v3.6 (R Core Team, 2017). Reads from cells isolated from PLHIV were aligned to the human genome (GRCh38), while reads from J1.1 T-cells were aligned to a custom reference consisting of the

599 genomic HIV-1 RNA (LAV-1, GenBank: K02013.1) appended to GRCh38 to allow for capture
600 of viral RNAs. The data was processed using the SCTransform workflow as outlined by the
601 Seurat developers. Cells were clustered using Louvain clustering in a UMAP projection. For
602 the $CD4^+$ T-cells from PLHIV, T-cell subsets were identified based on marker gene expression:
603 T_N cells ($CD3D^+$, $CD8A^-$, $CCR7^+$, $S100A4^{low}$) (39), T_{CM} cells ($CD3D^+$, $CD8A^-$, $CCR7^{low}$,
604 $S100A4^{int}$, $CD62L^{high}$, $GZMA^-$) (79), T_{TM} cells ($CD3D^+$, $CD8A^-$, $CCR7^{low}$, $S100A4^{high}$, $CD62L^{low}$,
605 $GZMA^+$, $GZMB^-$, $GZMH^-$, $PRF1^-$, $GNLY^+$) (80–82), T_{EM} cells ($CD3D^+$, $CD8A^-$, $CCR7^-$,
606 $S100A4^{high}$, $GZMA^+$, $GZMB^+$, $GZMH^+$, $PRF1^+$ $GNLY^+$) (83), T_{EMRA} cells ($CD3D^+$, $CD8A^-$, $CCR7^-$
607 , $S100A4^{high}$, $GZMA^+$, $GZMB^{high}$, $GZMH^+$, $PRF1^{high}$, $GNLY^{high}$, $CCL4^+$) (40,84), T_{REG} cells
608 ($CD3D^+$, $CD8A^-$, $CCR7^{low}$, $S100A4^{high}$, $FOXP3^+$, $IL2RA^+$, $CTLA4^+$) (40,84), T_{EX} cells ($CD3D^+$,
609 $CD8A^-$, $CCR7^-$, $GZMB^+$, $PDCD1^+$, $LAG3^+$) (85). All utilized code is deposited at
610 https://github.com/GoffinetLab/HIV_scRNAseq-CD4-LRA-study. To visualize sequencing
611 coverage of the viral genome in J1.1 T-cells, viral reads were extracted from the bam files of
612 the CellRanger output. These were converted to bigwig files and visualised on tracks using
613 bamCoverage (setting –normalizeUsing RPGC) and pyGenomeTracks from deeptools (86).
614

615 **Principal component analysis (PCA)**

616 PCA was performed with the average expression values of all genes with detectable
617 expression levels of mock-, Vorinostat- and Panobinostat-treated samples. Singular value
618 decomposition (SVD) with imputations was used for calculation of the principal components
619 using ClustVis (https://biit.cs.ut.ee/clustvis/) (87).
620

621 **Differentially expressed genes and pathway analysis**

622 DEGs between individual treatments were identified using the 10x Genomics Loupe Browser
623 (v. 5.0.1.); p-values were adjusted using the Benjamini-Hochberg correction for multiple
624 testing. Pathway analysis was performed with the list of DEGs harbouring p-values <0.05,
625 gene set enrichment analysis (GSEA) was performed using the Pathway Panther database
626 (88–90). The results are described using the Normalised Enrichment Ratio (NER), the

627 enrichment ratio indicates the degree of overrepresentation of a given gene set in the list of
628 DEGs and is normalised to take different gene set sizes into account.
629
630 **Transcription factor activity analysis**
631 Transcription factor activity analysis was performed using the dorothea R package following
632 the guidelines for processing single cell RNA-seq data (91,92), with the following exception.
633 The run_viper function from dorothea was altered to use the top 40,000 most variable genes,
634 as determined by the FindVariableFeatures function from Seurat. Utilised code is available at
635 https://github.com/GoffinetLab/HIV_scRNAseq-CD4-LRA-study.
636
637 **Module scores**
638 The IFN signalling pathway (R-HSA-913531) and TCR signalling pathway (R-HSA-202403)
639 gene sets from the Reactome database (93) were retrieved from the Molecular Signatures
640 Database (MSigDB) (94). Cells were scored based on their expression of these genes using
641 the AddModuleScore function in Seurat. They are referred to as the IFN signalling module and
642 T-cell activation module scores as the pathways include genes canonically involved in
643 response to IFN signalling and TCR-mediated T-cell activation, respectively.

644 **Flow cytometry**
645 PBS-washed cells were immunostained for individual surface proteins using the following
646 antibodies: anti-BST2/Tetherin-BV421 (#566381; BD), anti-CCR5/CD195-FITC (#555992; BD
647 Biosciences), anti-CCR7/CD197-PE (#552176; BD Biosciences), anti-CD107a-BV421
648 (#562623; BD), anti-CD14-PE (#555398; BD), anti-CD16-FITC (#360716; Biolegend), anti-
649 CD3-FITC (#561807; BD Biosciences), anti-CD4-APC (#555349; BD Biosciences), anti-
650 CD25-APC (#340907; BD Biosciences), anti-CD45RA-FITC (#335039; BD Biosciences), anti-
651 CD45RO-APC (#340438; BD Biosciences), anti-CD56-APC (#318310; Biolegend), anti-
652 CD62L-FITC (#304804; Biolegend), anti-CD69-APC (#340560; BD Biosciences), anti-
653 CXCR4/CD184-APC (#555976; BD Biosciences), anti-HLA-DR-FITC (#556643, BD

Biosciences), anti-IL7R/CD127-PE (#557938; BD), anti-PD-1/CD279-PE (#21272794; ImmunoTools) and anti-TIM-3/CD366-FITC (#345022; Biolegend). For intracellular immunostaining, PBS-washed cells were PFA-fixed for 90 minutes and immunostained with the following antibodies diluted in 0.1% Triton X-100 in PBS: anti-HIV-1-core-antigen-FITC or -PE (#6604665 or #6604667; Beckman Coulter), rabbit-anti-human-MX1/2 (#sc-166412; Santa Cruz Biotechnology). A goat-anti-rabbit IgG conjugated to Alexa Fluor 647 (#A27040; Thermo Fisher) was used as a secondary antibody. Cell viability was analysed using the Dead Cell Apoptosis Kit for Flow Cytometry from Invivogen (#V13242), with early apoptotic cells scoring Annexin V-positive and late apoptotic cells scoring Annexin V- and propidium iodide (PI)-positive. Data acquisition and analysis was conducted using a FACS Celesta device (Becton Dickinson, Franklin Lakes, New Jersey, USA) with FlowJo (v.10.7.1).

T-cell activation assays

$CD4^+$ T-cells were isolated from healthy donors and pre-incubated with Vorinostat (500 nM), Panobinostat (50 nM), or left mock-treated (0.05% DMSO) for 16 hours followed by stimulation with a peptide pool of a broad range of HLA-subtypes and infectious agents (CEFX Ultra SuperStim Pool; JPT) (1 µg/ml) and 1 µg/ml mouse-anti-human CD28 antibody (#556620; BD Biosciences), or IL-2 (20 IU/ml) and PHA (1 µg/ml). T-cell activation and exhaustion was quantified by flow cytometry 48 hours post-stimulation.

HIV-1 reactivation assays in J1.1 T-cells

J1.1 T-cells were PBS-washed, resuspended in supplemented RPMI and incubated with Panobinostat (50 nM), Vorinostat, (5000 nM), Romidepsin (50 nM), Bryostatin (20 nM), JQ1 (5000 nM) or the corresponding volume of DMSO, if not otherwise stated for 48 hours. In some assays, T-cells were co-treated or pre-treated for 24 hours with individual IFNs at indicated concentrations.

Quantitative RT-Q-PCR

Total RNA extraction using the Direct-zol RNA extraction kit (Zymo) including DNase treatment to remove residual DNA contaminations, was followed by cDNA synthesis (NEB, Invitrogen) and quantification of relative mRNA levels using a LightCycler 480 Instrument II (Roche) and Taq-Man PCR technology. For human *IFIT1* and *MX2*, a premade primer-probe kit was purchased from Applied Biosystems (Assay ID: Hs01911452_s1; Hs01550813_m1; respectively. Relative mRNA levels were determined in multiplex reactions using the ΔΔCt method and human *RNASEP* (#4316844; Applied Biosystems) as internal reference. Data analysis was performed using LightCycler Software 4.1 (Roche).

Immunoblotting

For immunoblotting, cells were lysed using the M-PER mammalian protein extraction reagent (Thermo Fisher Scientific) following manufacturer's recommendations. Cell cultures supernatants were centrifuged over a 20% sucrose cushion at 20,000 x g, for 60 mins at 4°C, resuspended in 1x SDS buffer at heat-inactivated for 10 mins at 95°C. Samples were run on a 10% SDS-PAGE, transferred onto nitrocellulose membranes using a semi-dry transfer system (Bio-Rad Laboratories) and membranes were blocked with 5% milk in TBS for one hour before incubation with the primary antibody at 4°C overnight. The following primary antibodies were used: anti-90K/LGALS3BP (#AF2226: R&D Systems), anti-BST2/Tetherin (#390719; Santa Cruz), anti-ERK2/MAPK (#sc-153; Santa Cruz) anti-GAPDH (#NB300-221, Novus Biologicals), anti-HIV-1 p24 (#11-327; ExBio), anti-HIV-1 gp120 (provided by Valerie Bosch), anti-IFIT1 (#TA500948; OriGene), anti-IFITM-3 (#AP1153a; Abgent), anti-ISG15 (#166755; Santa Cruz) and anti-MX2 (#sc166412; Santa Cruz). Secondary antibodies conjugated to Alexa680 or Alexa800 fluorescent dyes were used for detection and quantification by the Odyssey Infrared Imaging System (LI-COR Biosciences).

Release of HIV-1 p24 capsid was quantified by detecting p24 as described above in supernatant and cell samples from corresponding cell cultures and dividing the p24 signal intensity from supernatants by the sum of p24 intensities from both fractions.

Tzm-bl HIV-1 infectivity assay

To quantify infectivity released in supernatant, 30,000 Tzm-bl cells per 96-well were pre-treated with 10 µM of the JAK/STAT inhibitor Ruxolitinib for 16 hours to minimise the influence of potentially transferred IFNs from the tested supernatants. Then, cells were infected with HIV-1 for 48 hours before luminometric quantification of luciferase activity using the Luciferase Assay System (Promega).

HIV-1 Env cell surface staining

To quantify HIV-1 Env cell surface expression, broadly neutralising antibodies 3BNC117 (ARP-12474), 10-1074 (ARP-12477) and PG16 (ARP-12150) were obtained from the NIH HIV Reagents Program. PBS-washed cells were immunostained with a cocktail of 5 µg/ml of each antibody for 30 mins at 4°C, followed by PBS washing and immunostaining with secondary AlexaFluor633 anti-human antibodies (Thermo Fisher Scientific, #A-21091) for 30 mins at 4°C in the dark. Samples were PBS-washed and fixed with 4% PFA for 90 minutes. Samples were acquired and analysed on a FACS Celesta machine (BD Biosciences) and FlowJo Software (V.10.7.1), respectively.

Thin section electron microscopy

Infected T-cells were fixed with 2.5% glutaraldehyde in 0.05 M Hepes buffer (pH:7.2) and incubated at room temperature for two hours. Afterwards, µ-Dishes were filled with the fixative buffer and cells were embedded in the chambers by using Epon resin (protocol with tannic acid and uranyl acetate block contrasting (95). Thin sections (60-70 nm thick) were produced with an ultramicrotome, contrasted with uranyl acetate and lead citrate and investigated with a transmission electron microscope (JEM-2100, Jeol) operated at 200 kV. Images were recorded using a side-mounted CCD camera (Veleta, EMSIS) with 2048x2048 pixels.

735 **Antibody-dependent cellular cytotoxicity (ADCC) assay**

736 ADCC assays were adapted from previous reports (96). Briefly, J1.1 T-cells were treated as
737 described above for 48 hours, before washing and staining with green CellTracker (#C2925,
738 Thermo Fisher Scientific), following manufacturer's recommendations. Labelled J1.1 T-cells
739 were then co-cultured with freshly isolated PBMCs (or NK cells or monocytes where indicated)
740 at a 1:1 ratio in a 96-well U-bottom plate in the presence of indicated dilutions of serum from
741 PLHIV (ARP-3957; obtained from the NIH HIV Reagents Program). A separate well without
742 serum was set up for each co-culture condition in parallel. The plates were then centrifuged
743 for one min, 300 x *g* and then incubated at 37°C, 5% CO_2. After four hours, co-cultures were
744 PBS-washed, fixed with 4% PFA, immunostained for intracellular HIV-1 p24 expression and
745 p24 CA-positive J1.1 T-cells were quantified by flow cytometry. Percent of ADCC was
746 calculated using this formula (see also **Sup. Fig. 8**):

747 $$\%\ ADCC$$

748 $$= \frac{p24-positive\ J1.1\ cells\ (without\ sera)\ -\ p24-positive\ J1.1\ cells\ (with\ sera)}{p24-positive\ J1.1\ cells\ (without\ sera)}\ x\ 100$$

749

750 **NK cell activation and CD107a degranulation assay**

751 NK cell activation and degranulation activity in PBMCs co-cultured with reactivated J1.1 T-
752 cells was analysed through CD16 and CD107a immunostaining of NK cells. ADCC assays
753 were performed as described above with the following modifications (97): Co-cultures were
754 supplemented with a 1:20 dilution of anti-CD107a-BV421 antibodies. After one hour of
755 incubation, a final concentration of 10 µg/ml Brefeldin A and 6 µg/ml Golgi-Stop (BD
756 Biosciences) were added, preventing the exocytosis of cytokine-containing vesicles, and the
757 acidification of endocytic vesicles and CD107a protein degradation, respectively. Co-cultures
758 were incubated for another three hours at 37°C, 5% CO_2, before immunostaining for CD16
759 and CD56 cell surface expression. CD16 and CD107a expression was assessed by flow
760 cytometry specifically in CD56-positive NK cell populations (see also **Sup Fig. 9**).

761

762 **Live-cell imaging of J1.1 T-cell/NK cell co-cultures**

763 To analyse the dynamics of NK cell-mediated ADCC against reactivating J1.1 T-cells, live cell
764 imaging of indicated co-cultures was performed. J1.1 T-cell cultures treated with Panobinostat
765 or Panobinostat/IFN-α2a for 48 hours were individually labelled with CellTracker™ Green-
766 CFMDA or CellTracker™ Deep Red CellTracker (both Thermo Fisher Scientifics).
767 Panobinostat-treated, Panobinostat/IFN-α2a-treated J1.1 T-cells and NK cells were co-
768 cultured at a 1:1:1 ratio in the presence of 1:100 dilution of sera from PLHIV and the
769 LIVE/DEAD Aqua Dead Cell dye (Thermo Fisher Scientific, #L34965) to assess dying cells.
770 The dead cell dye reacts with free amids in the cellular cytosol, thus specifically staining cells
771 with porous membranes as an early surrogate of cell death. Co-cultures were monitored with
772 a Zeiss LSM800 Airyscan Confocal Microscope in a 37°C, 5% CO_2 atmosphere with images
773 being acquired every three minutes for a total of four hours. Images were analysed and
774 merged using Zeiss ZEN Blue (V3.3).
775

776 **Data presentation and statistical analysis**

777 Graphs and figures were generated using Graphpad Prism 9 (v.9.5.1) and Adobe Illustrator
778 2021. Heatmaps were generated using the ClustVis web tool (https://biit.cs.ut.ee/clustvis/)
779 with unit variance scaling for rows (87). If not otherwise stated, bars or circles represent the
780 mean of the indicated number of experiments and error bars indicate the S.E.M. Statistical
781 significance for paired data sets were tested using Graphpad Prism 9 and paired student's t-
782 testing, p-values ≤ 0.05 were considered significant and displayed in the figures as follows: p
783 < 0.05 *; p < 0.01 ** or p < 0.001 ***. p-values ≥ 0.05 were considered not significant (n.s.).
784 Pearson's correlation analyses were performed for the indicated datasets with pearson
785 correlation coefficients and two-tailed p-values being displayed.

786 **Data availability**

The single cell RNA-sequencing data will be deposited at the Gene Expression Omnibus (GEO) database (accession number #).

ACKNOWLEDGEMENTS

We thank the PLHIV who agreed to participate in the Seroconverter Study and the uninfected donors to provide their blood for research. We thank Valerie Bosch and the NIH AIDS Research & Reference Reagent Program for providing essential reagents. We thank the Genomics Platform of the Berlin Institute of Health for next-generation sequencing. This work was supported by funding to C.G. by Berlin Institute of Health (BIH); by Hector Foundation, project M2101; by DFG priority program 1923 “Innate Sensing and Restriction of Retroviruses,” grant GO2153/4); by DZIF, TTU HIV, grant 04.820 to C.G. and by a Professorship Award (APR9/1017) of the Academy of Medical Sciences awarded to C.G. We thank Christian Drosten for constant support. A.P. is supported by the Brazilian Federal Foundation for Support and Evaluation of Graduate Education, CAPES. J.K. is supported by the Center of Infection Biology and Immunity (ZIBI) and Charité PhD Program.

AUTHOR CONTRIBUTIONS

JP, AJP, JJ, LM, JF, TS, performed experiments.

JP, DP, AJP, EW, LM, JF, TS, CF, SV, MS analysed data.

UK, BGB, KM, NB, LL, AT, KS provided essential resources.

AT, SS, UD, MiL, NB, MaL, CG supervised.

CG acquired funding and managed the project.

JP, DP, CG wrote the manuscript.

Declaration of conflicts of interest

None.

812 **FIGURES**

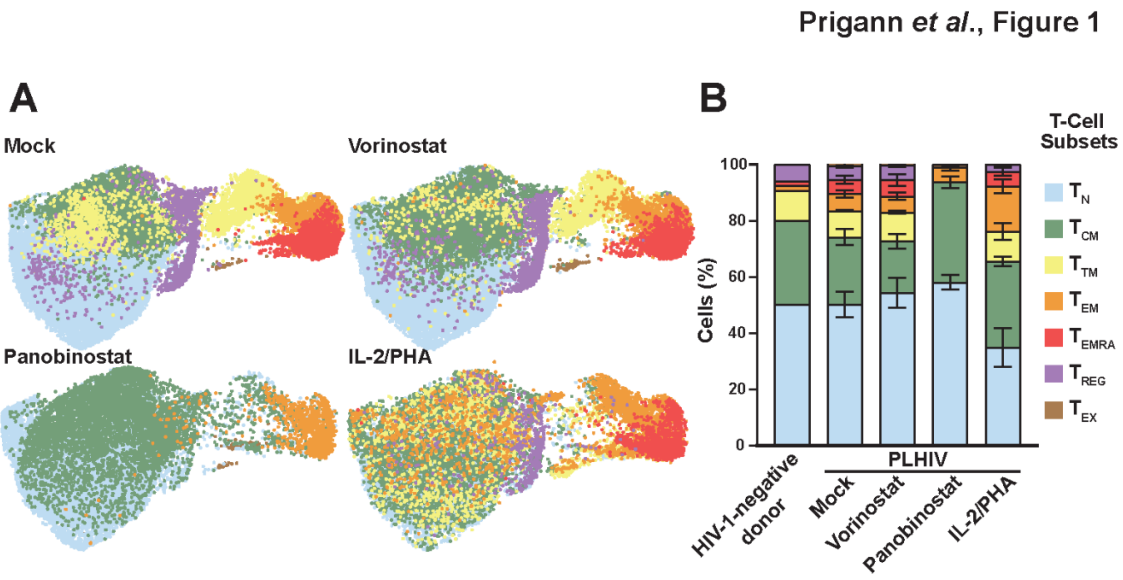

813

814 **Figure 1. Panobinostat treatment modulates expression of CD4⁺ T-cell subset-specific**

815 **markers**

816 (**A**) Combined UMAP plot of CD4⁺ T-cell cultures from three PLHIV, separated by treatment

817 and coloured by T-cell subset.

818 (**B**) Percentages of indicated CD4⁺ T-cell subsets.

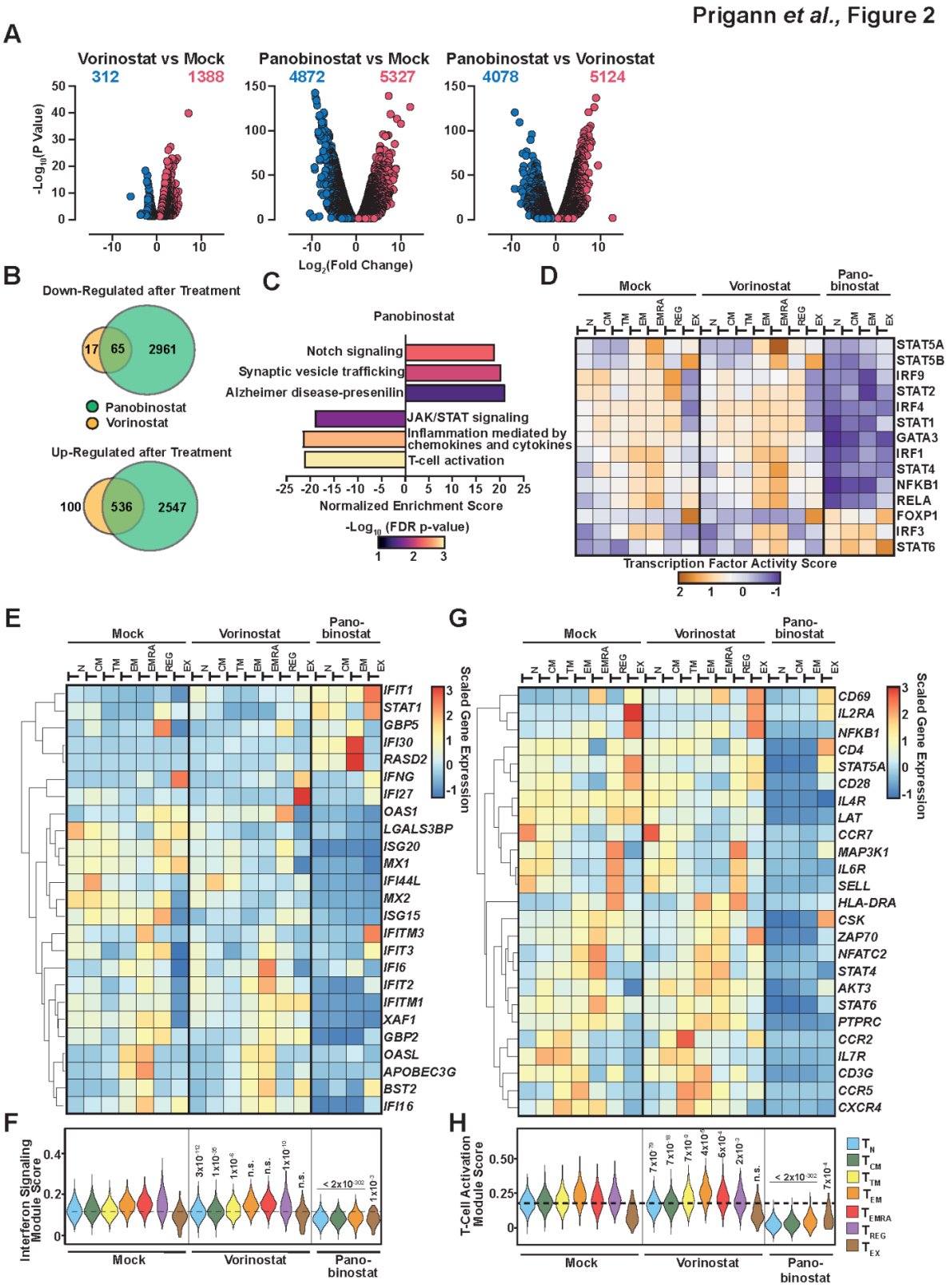

Figure 2. Panobinostat treatment induces broad transcriptional down-modulation of genes involved in T-cell signalling and a subset of genes implicated in innate immunity

(**A**) Volcano plots showing DEGs with a p-value < 0.05.

(**B**) Overlap of genes significantly up- or down-regulated (p-value < 0.05, fold change > 2) in Vorinostat and Panobinostat-treated samples compared to mock treatment.

(**C**) Pathway analysis of DEGs (p-value < 0.05) after Panobinostat treatment. Shown is the Normalised Enrichment Ration (NER), representing the degree of overrepresentation of a given gene set in the DEG list. Colours indicate the $-Log_{10}$(FDR p-value).

(**D**) Transcription factor activity analysis of selected transcription factors in the indicated T-cell subsets.

(**E**) Heatmap showing scaled average expression of selected ISGs in the indicated T-cell subsets. Genes are ordered based on correlation, clustering is indicated with lines on the left.

(**F**) Average IFN signalling module score in the indicated T-cell subsets. Dashed line shows the average module score of mock-treated T_N-cells. Numbers indicate the p-value calculated using Wilcoxon signed-rank testing for each subset from the LRA-treated samples compared to the same subset of the mock-treated samples.

(**G**) Heatmap showing scaled average expression of selected genes required for T-cell-mediated immunity in the indicated T-cell subsets. Genes are ordered based on correlation, clustering is indicated with lines on the left.

(**H**) Average T-cell activation module score in the indicated T-cell subsets. Dashed line shows the average module score of mock-treated T_N-cells. Numbers indicate the p-value calculated using Wilcoxon signed-rank testing for each subset from the LRA-treated samples compared to the same subset of the mock-treated samples.

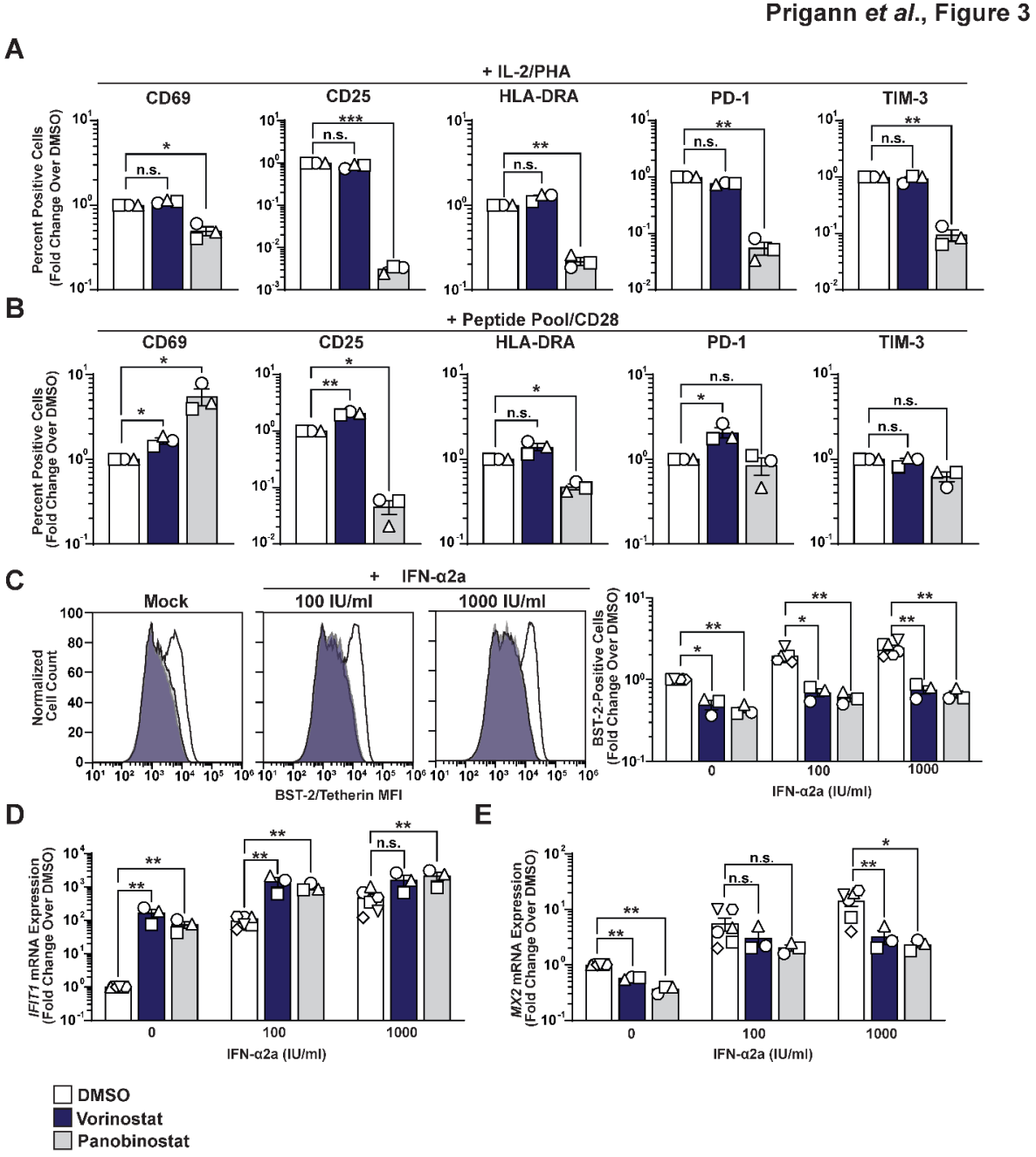

Figure 3. HDAC inhibition imposes a block to CD4⁺ T-cell activation and type I IFN signalling

CD4⁺ T-cells from uninfected donors were either pretreated with 0.5% DMSO, 500 nM Vorinostat or 50 nM Panobinostat for 16 hours, followed by:

(**A**) Stimulation with a peptide pool and anti-CD28 antibody for 48 hours

(**B**) Stimulation with IL-2/PHA for 48 hours

851 followed by analysis of CD69, CD25, HLA-DR, TIM-3 and PD-1 cell surface expression by flow
852 cytometry. Shown are data from cells from three donors.
853 $CD4^+$ T-cells from uninfected donors were treated with 0.5% DMSO, 8000 nM Vorinostat or
854 50 nM Panobinostat in combination with increasing concentrations of IFN-α2a for 48 hours
855 before analysing:
856 (**C**) BST2 cell surface levels by flow cytometry. Shown are representative histograms from one
857 experiment (left panel) and quantification from experiments with cells from three donors.
858 (**D**) *IFIT1* mRNA expression by RT-Q-PCR. Shown are data from cells from 3-6 donors.
859 (**E**) *MX2* mRNA expression by RT-Q-PCR. Shown are data from cells from 3-6 donors.
860
861
862

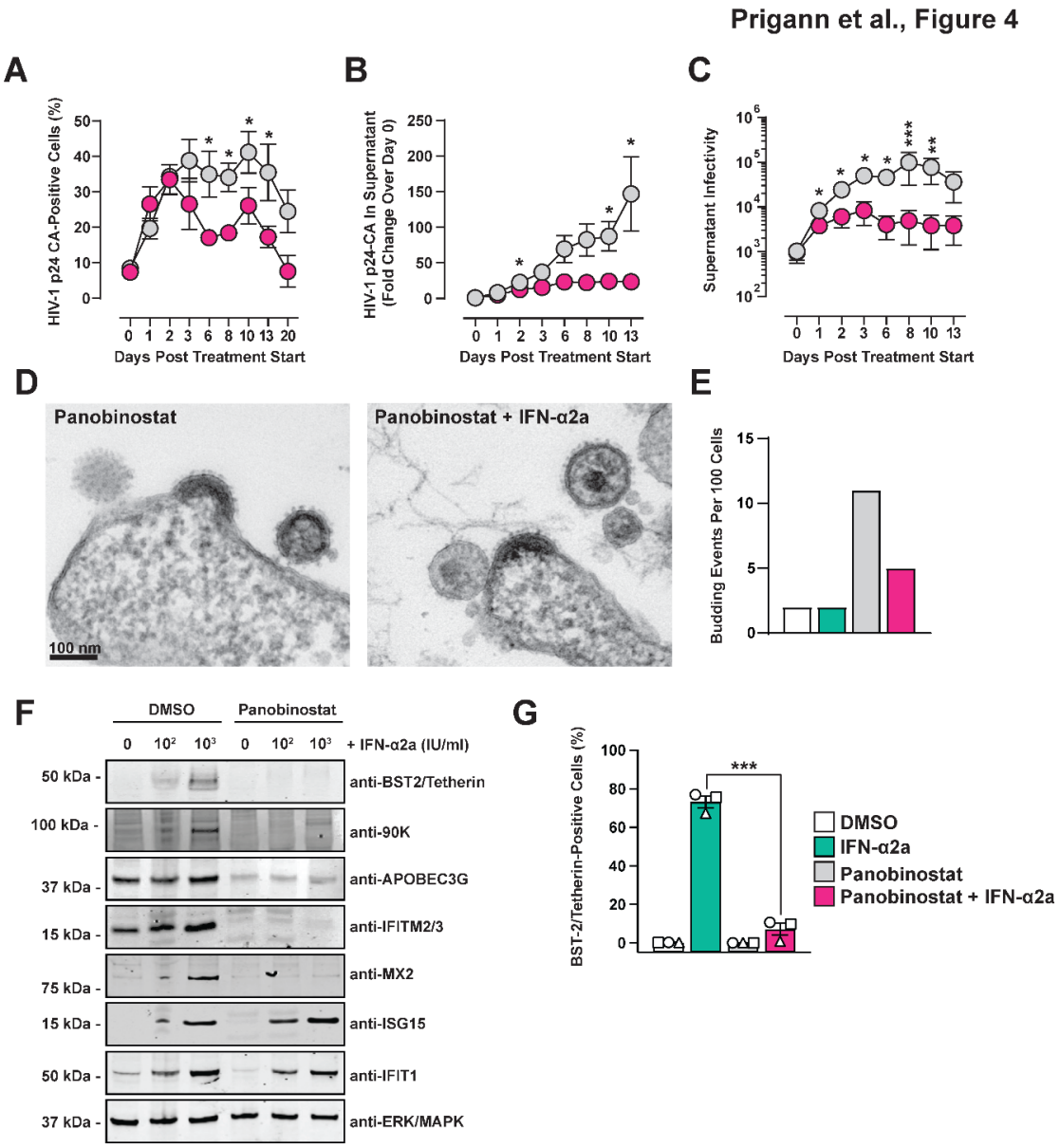

Figure 4. Addition of IFN-α2a to Panobinostat results in a tetherin-independent pre-budding defect

J1.1 T-cells received a single dose of 50 nM Panobinostat alone or in combination with 100 IU/ml IFN-α2a. At indicated time points, samples were analysed for:

(**A**) Cell-associated HIV-1 p24 capsid expression by flow cytometry

(**B**) HIV-1 p24 capsid abundance in cell culture supernatant by immunoblotting.

(**C**) Infectivity in cell culture supernatant using the Tzm-bl reporter cell assay.

(**D**) Representative electron micrographs of reactivated J1.1 T-cells 48 hours post reactivation. Scale bar indicates 100 nm.

873 (**E**) Electron microscopy-based quantification of budding events per 100 cells analysed.

874 (**F**) Immunoblot analysis of selected ISG expression in J1.1 T-cells following 48 hours of

875 indicated treatment.

876 (**G**) J1.1 T-cell surface BST-2/Tetherin expression 48 hours following treatment start.

877

878

879

880

881

882

883

884

885

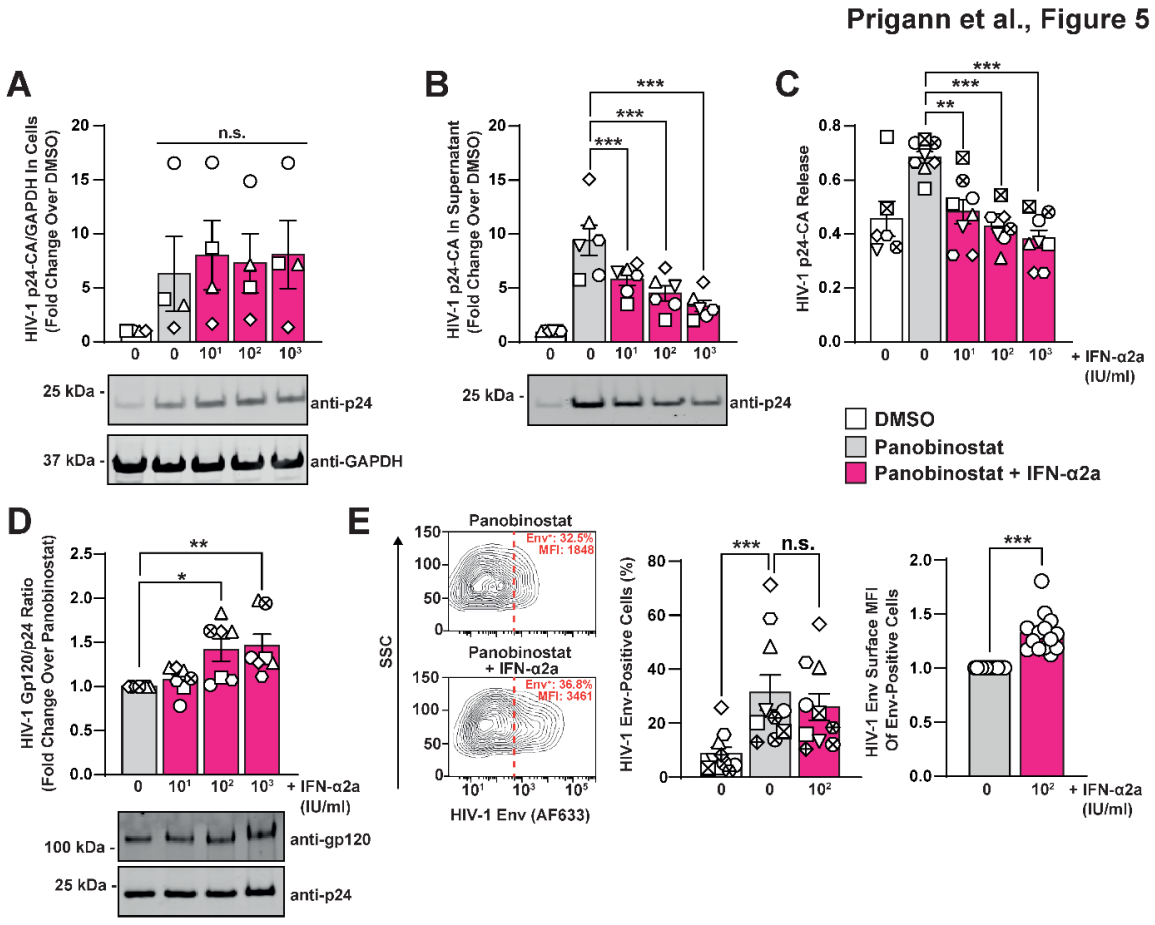

886

887 **Figure 5. IFN-induced virus pre-budding block is accompanied by accumulation of HIV-**
888 **1 Env on cellular and viral membranes**
889 J1.1 T-cells were treated with 50 nM Panobinostat in the presence or absence of indicated
890 concentrations of IFN-α2a for 48 hours. Cells and corresponding supernatants were analysed
891 for:
892 (**A**) Relative expression of cell-associated HIV-1 p24-CA by immunoblotting, normalised to
893 cellular GAPDH.
894 (**B**) Relative abundance of extracellular HIV-1 p24-CA by immunoblotting, normalised to
895 corresponding DMSO controls.
896 (**C**) Virus release was quantified by normalising extracellular HIV-1 p24-CA signal intensity to
897 the sum of cell-associated and secreted HIV-1 p24-CA.
898 (**D**) HIV-1 gp120 signal intensities from cell culture supernatants were quantified by
899 immunoblotting and normalised to corresponding HIV-1 p24-CA levels.
900 (**E**) Representative dot plots of intact J1.1 T-cells immunostained for surface HIV-1 Env with
901 indicated percentage of Env-positive cells and mean fluorescence intensity (MFI) of Env-
902 positive cells. Quantification of HIV-1 Env-positive cells (middle) and the fold change of Env
903 MFI in Env-positive cells over Panobinostat-treated cells (right) are shown for multiple
904 experimental replicates.
905 Experiments were conducted in 5-13 independent replicates.
906
907
908
909
910
911
912
913
914

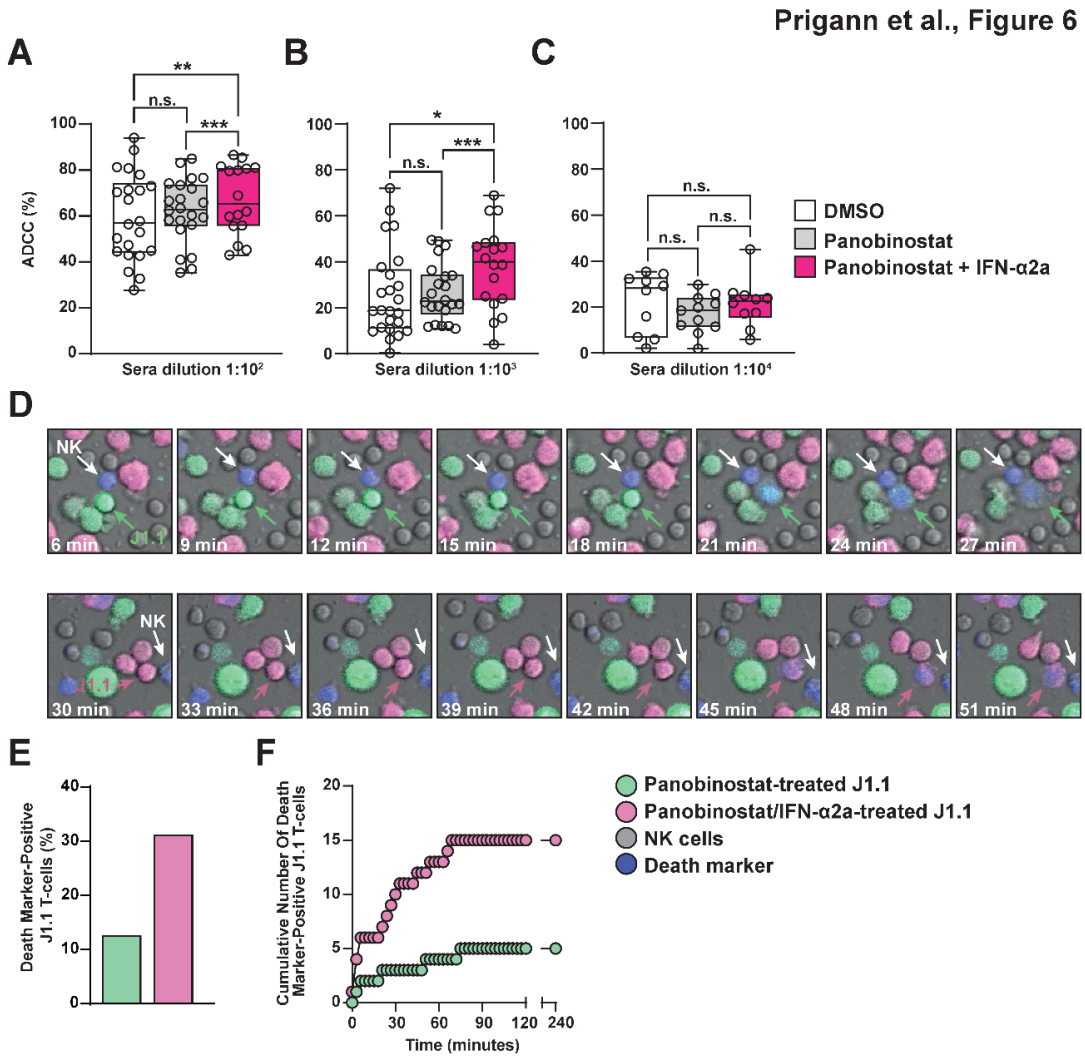

Figure 6. Addition of IFN-α2a to Panobinostat enhances the susceptibility of HIV-1-reactivating cells to antibody-dependent cellular cytotoxicity via NK cells

(**A-C**) J1.1 T-cells were treated with DMSO, 50 nM Panobinostat alone or in combination with 100 IU/ml IFN-α2a for 48 hours before culturing them with PBMCs in the presence of indicated dilutions of sera from PLHIV. Following four hours of co-culture, cells were immunostained for cell-associated HIV-1 p24 CA expression and percentage of ADCC was calculated based on the quantitative difference of HIV-1-p24-positive cells in the identical co-culture merely differing in the presence or absence of serum. Boxes extend from the 25th to 75th percentiles of 10-24 repetitions, the lines indicate the median, error bars represent the minimum and maximum values obtained and symbols the individual experimental replicates.

(**D**) - (**F**) J1.1 T-cells were treated with 50 nM Panobinostat alone or in combination with 100 IU/ml IFN-α2a for 48 hours and individually stained with CellTracker™ Green-CFMDA and Deep Red, respectively. Stained J1.1 T-cells were co-cultured with non-stained, freshly isolated NK cells at a 1:1:1 ratio in the presence of a cell death marker (blue) and a 1:100 dilution of sera from PLHIV containing anti-HIV-1 Env antibodies. The co-culture was monitored using live-cell imaging for four hours with images acquired every three minutes.

(**D**) Representative time series of NK cell/J1.1 T-cell interactions and subsequent killing of J1.1 T-cells.

(**E**) Percentage of dead J1.1 T-cells after four hours, normalised to the number of living J1.1 T-cells in the first frame.

(**F**) Cumulative number of death marker-positive cells in each J1.1 T-cell population over time.

954

955

956

957

958

959

960

Prigann et al., Figure 7

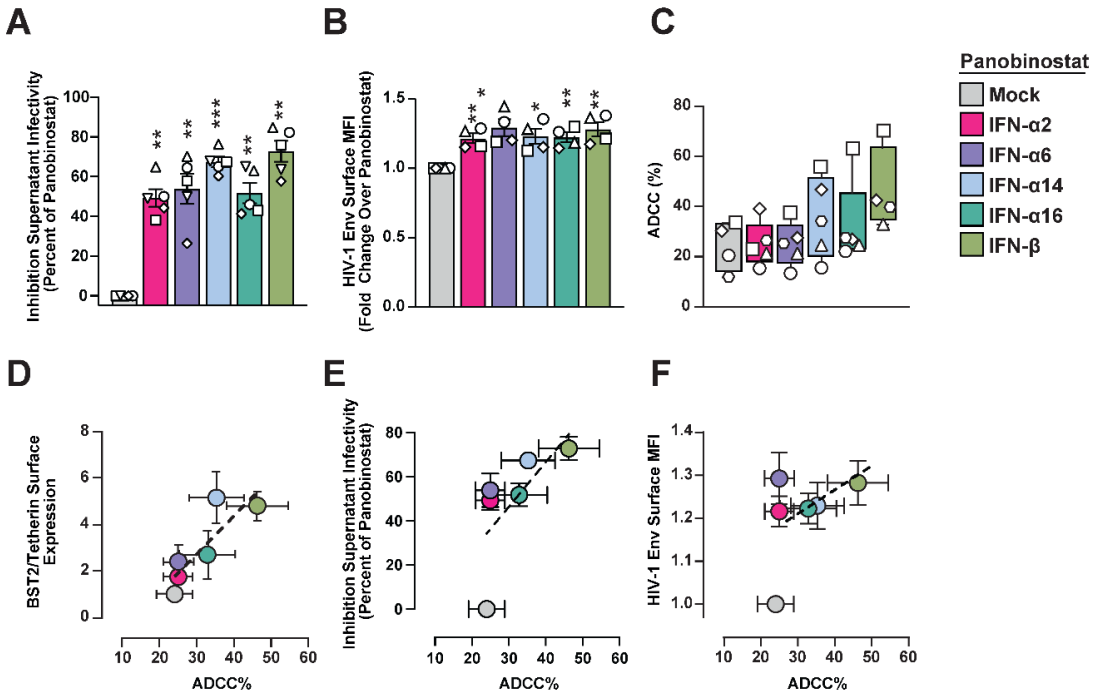

961

962 **Figure 7. The ability to restrict HIV-1 budding and facilitate elimination of HIV-1-positive**

963 **T-cells is type I IFN protein-specific**

964

965 J1.1 T-cells were treated with 50 nM Panobinostat in combination with 100 IU/ml of the

966 indicated IFNs for 48 hours.

967 (**A**) Inhibition of supernatant infectivity was quantified using a Tzm-bl reporter assay, values

968 were normalised to the corresponding Panobinostat-only conditions.

969 (**B**) Fold change of Env MFI in Env-positive cells over Panobinostat-treated cells.

(**C**) J1.1 T-cells were co-cultured with PBMCs in the presence of serum from PLHIV (dilution 1:1000) to monitor and quantify ADCC.

(**D**) - (**F**) Pearson's correlation analysis of ADCC % with BST2/Tetherin surface expression, supernatant infectivity and HIV-1 Env surface expression levels.

REFERENCES

1. Chun TW, Carruth L, Finzi D, Shen X, DiGiuseppe JA, Taylor H, et al. Quantification of latent tissue reservoirs and total body viral load in HIV-1 infection. Nature. 1997 May 8;387(6629):183–8.
2. Chun TW, Stuyver L, Mizell SB, Ehler LA, Mican JA, Baseler M, et al. Presence of an inducible HIV-1 latent reservoir during highly active antiretroviral therapy. Proc Natl Acad Sci U S A. 1997 Nov 25;94(24):13193–7.
3. Finzi D, Hermankova M, Pierson T, Carruth LM, Buck C, Chaisson RE, et al. Identification of a reservoir for HIV-1 in patients on highly active antiretroviral therapy. Science. 1997 Nov 14;278(5341):1295–300.
4. Wong JK, Hezareh M, Günthard HF, Havlir DV, Ignacio CC, Spina CA, et al. Recovery of replication-competent HIV despite prolonged suppression of plasma viremia. Science. 1997 Nov 14;278(5341):1291–5.
5. Finzi D, Blankson J, Siliciano JD, Margolick JB, Chadwick K, Pierson T, et al. Latent infection of CD4+ T cells provides a mechanism for lifelong persistence of HIV-1, even in patients on effective combination therapy. Nat Med. 1999 May;5(5):512–7.
6. Siliciano JD, Kajdas J, Finzi D, Quinn TC, Chadwick K, Margolick JB, et al. Long-term follow-up studies confirm the stability of the latent reservoir for HIV-1 in resting CD4+ T cells. Nat Med. 2003 Jun;9(6):727–8.
7. Deeks SG, Archin N, Cannon P, Collins S, Jones RB, de Jong MAWP, et al. Research priorities for an HIV cure: International AIDS Society Global Scientific Strategy 2021. Nat Med. 2021 Dec;27(12):2085–98.
8. Kim Y, Anderson JL, Lewin SR. Getting the "kill" into "shock and kill": strategies to eliminate latent HIV. Cell Host Microbe. 2018 Jan 10;23(1):14–26.
9. Margolis DM, Garcia JV, Hazuda DJ, Haynes BF. Latency reversal and viral clearance to cure HIV-1. Science. 2016 Jul 22;353(6297):aaf6517.
10. Van Lint C, Emiliani S, Ott M, Verdin E. Transcriptional activation and chromatin remodeling of the HIV-1 promoter in response to histone acetylation. EMBO J. 1996 Mar 1;15(5):1112–20.
11. Archin NM, Keedy KS, Espeseth A, Dang H, Hazuda DJ, Margolis DM. Expression of latent human immunodeficiency type 1 is induced by novel and selective histone deacetylase inhibitors. AIDS. 2009 Sep 10;23(14):1799–806.
12. Søgaard OS, Graversen ME, Leth S, Olesen R, Brinkmann CR, Nissen SK, et al. The Depsipeptide Romidepsin Reverses HIV-1 Latency In Vivo. PLoS Pathog. 2015 Sep;11(9):e1005142.
13. Williams SA, Chen LF, Kwon H, Fenard D, Bisgrove D, Verdin E, et al. Prostratin antagonizes HIV latency by activating NF-kappaB. J Biol Chem. 2004 Oct 1;279(40):42008–17.

14. Beans EJ, Fournogerakis D, Gauntlett C, Heumann LV, Kramer R, Marsden MD, et al. Highly potent, synthetically accessible prostratin analogs induce latent HIV expression in vitro and ex vivo. Proc Natl Acad Sci. 2013 Jul 16;110(29):11698–703.
15. Gutiérrez C, Serrano-Villar S, Madrid-Elena N, Pérez-Elías MJ, Martín ME, Barbas C, et al. Bryostatin-1 for latent virus reactivation in HIV-infected patients on antiretroviral therapy. AIDS Lond Engl. 2016 Jun 1;30(9):1385–92.
16. Zhu J, Gaiha GD, John SP, Pertel T, Chin CR, Gao G, et al. Reactivation of latent HIV-1 by inhibition of BRD4. Cell Rep. 2012 Oct 25;2(4):807–16.
17. Nixon CC, Mavigner M, Sampey GC, Brooks AD, Spagnuolo RA, Irlbeck DM, et al. Systemic HIV and SIV latency reversal via non-canonical NF-κB signalling in vivo. Nature. 2020 Feb;578(7793):160–5.
18. Thibault S, Imbeault M, Tardif MR, Tremblay MJ. TLR5 stimulation is sufficient to trigger reactivation of latent HIV-1 provirus in T lymphoid cells and activate virus gene expression in central memory CD4+ T cells. Virology. 2009 Jun 20;389(1–2):20–5.
19. Novis CL, Archin NM, Buzon MJ, Verdin E, Round JL, Lichterfeld M, et al. Reactivation of latent HIV-1 in central memory CD4$^+$ T cells through TLR-1/2 stimulation. Retrovirology. 2013 Oct 24;10:119.
20. Abner E, Jordan A. HIV “shock and kill” therapy: In need of revision. Antiviral Res. 2019 Jun;166:19–34.
21. Arandjelovic P, Kim Y, Cooney JP, Preston SP, Doerflinger M, McMahon JH, et al. Venetoclax, alone and in combination with the BH3 mimetic S63845, depletes HIV-1 latently infected cells and delays rebound in humanized mice. Cell Rep Med. 2023 Sep 19;4(9):101178.
22. Collins DR, Gaiha GD, Walker BD. CD8+ T cells in HIV control, cure and prevention. Nat Rev Immunol. 2020 Aug;20(8):471–82.
23. Lambotte O, Pollara J, Boufassa F, Moog C, Venet A, Haynes BF, et al. High antibody-dependent cellular cytotoxicity responses are correlated with strong CD8 T cell viral suppressive activity but not with B57 status in HIV-1 elite controllers. PloS One. 2013;8(9):e74855.
24. Madhavi V, Wines BD, Amin J, Emery S, ENCORE1 Study Group, Lopez E, et al. HIV-1 Env- and Vpu-Specific Antibody-Dependent Cellular Cytotoxicity Responses Associated with Elite Control of HIV. J Virol. 2017 Sep 15;91(18):e00700-17.
25. Rerks-Ngarm S, Pitisuttithum P, Nitayaphan S, Kaewkungwal J, Chiu J, Paris R, et al. Vaccination with ALVAC and AIDSVAX to prevent HIV-1 infection in Thailand. N Engl J Med. 2009 Dec 3;361(23):2209–20.
26. Haynes BF, Gilbert PB, McElrath MJ, Zolla-Pazner S, Tomaras GD, Alam SM, et al. Immune-correlates analysis of an HIV-1 vaccine efficacy trial. N Engl J Med. 2012 Apr 5;366(14):1275–86.
27. Tomescu C, Tebas P, Montaner LJ. IFN-α augments natural killer-mediated antibody-dependent cellular cytotoxicity of HIV-1-infected autologous CD4+ T cells regardless of major histocompatibility complex class 1 downregulation. AIDS Lond Engl. 2017 Mar 13;31(5):613–22.
28. Tomescu C, Chehimi J, Maino VC, Montaner LJ. NK cell lysis of HIV-1-infected autologous CD4 primary T cells: requirement for IFN-mediated NK activation by plasmacytoid dendritic cells. J Immunol Baltim Md 1950. 2007 Aug 15;179(4):2097–104.
29. Azzoni L, Foulkes AS, Papasavvas E, Mexas AM, Lynn KM, Mounzer K, et al. Pegylated Interferon alfa-2a monotherapy results in suppression of HIV type 1 replication and decreased cell-associated HIV DNA integration. J Infect Dis. 2013 Jan 15;207(2):213–22.
30. Papasavvas E, Azzoni L, Pagliuzza A, Abdel-Mohsen M, Ross BN, Fair M, et al. Safety, Immune, and Antiviral Effects of Pegylated Interferon Alpha 2b Administration in Antiretroviral Therapy-Suppressed Individuals: Results of Pilot Clinical Trial. AIDS Res Hum Retroviruses. 2021 Jun;37(6):433–43.
31. Hua S, Vigano S, Tse S, Zhengyu O, Harrington S, Negron J, et al. Pegylated Interferon-α-Induced Natural Killer Cell Activation Is Associated With Human Immunodeficiency

Virus-1 DNA Decline in Antiretroviral Therapy-Treated HIV-1/Hepatitis C Virus-Coinfected Patients. Clin Infect Dis Off Publ Infect Dis Soc Am. 2018 Jun 1;66(12):1910–7.

32. Boué F, Reynes J, Rouzioux C, Emilie D, Souala F, Tubiana R, et al. Alpha interferon administration during structured interruptions of combination antiretroviral therapy in patients with chronic HIV-1 infection: INTERVAC ANRS 105 trial. AIDS Lond Engl. 2011 Jan 2;25(1):115–8.
33. Papasavvas E, Azzoni L, Kossenkov AV, Dawany N, Morales KH, Fair M, et al. NK Response Correlates with HIV Decrease in Pegylated IFN-α2a-Treated Antiretroviral Therapy-Suppressed Subjects. J Immunol Baltim Md 1950. 2019 Aug 1;203(3):705–17.
34. Jiao Y mei, Weng W jia, Gao Q sheng, Zhu W jun, Cai W ping, Li L hua, et al. Hepatitis C therapy with interferon-α and ribavirin reduces the CD4 cell count and the total, 2LTR circular and integrated HIV-1 DNA in HIV/HCV co-infected patients. Antiviral Res. 2015 Jun;118:118–22.
35. Hurst J, Hoffmann M, Pace M, Williams JP, Thornhill J, Hamlyn E, et al. Immunological biomarkers predict HIV-1 viral rebound after treatment interruption. Nat Commun. 2015 Dec;6(1):8495.
36. Archin NM, Liberty AL, Kashuba AD, Choudhary SK, Kuruc JD, Crooks AM, et al. Administration of vorinostat disrupts HIV-1 latency in patients on antiretroviral therapy. Nature. 2012 Jul 25;487(7408):482–5.
37. Rasmussen TA, Tolstrup M, Brinkmann CR, Olesen R, Erikstrup C, Solomon A, et al. Panobinostat, a histone deacetylase inhibitor, for latent-virus reactivation in HIV-infected patients on suppressive antiretroviral therapy: a phase 1/2, single group, clinical trial. Lancet HIV. 2014 Oct;1(1):e13-21.
38. Rasmussen TA, Søgaard OS, Brinkmann C, Wightman F, Lewin SR, Melchjorsen J, et al. Comparison of HDAC inhibitors in clinical development: Effect on HIV production in latently infected cells and T-cell activation. Hum Vaccines Immunother. 2013 May 14;9(5):993–1001.
39. Mahnke YD, Brodie TM, Sallusto F, Roederer M, Lugli E. The who's who of T-cell differentiation: Human memory T-cell subsets: HIGHLIGHTS. Eur J Immunol. 2013 Nov;43(11):2797–809.
40. Cano-Gamez E, Soskic B, Roumeliotis TI, So E, Smyth DJ, Baldrighi M, et al. Single-cell transcriptomics identifies an effectorness gradient shaping the response of CD4+ T cells to cytokines. Nat Commun. 2020 Dec;11(1):1801.
41. Szabo PA, Levitin HM, Miron M, Snyder ME, Senda T, Yuan J, et al. Single-cell transcriptomics of human T cells reveals tissue and activation signatures in health and disease. Nat Commun. 2019 Dec;10(1):4706.
42. Breton G, Chomont N, Takata H, Fromentin R, Ahlers J, Filali-Mouhim A, et al. Programmed Death-1 Is a Marker for Abnormal Distribution of Naive/Memory T Cell Subsets in HIV-1 Infection. J Immunol. 2013 Sep 1;191(5):2194–204.
43. Wang S, Zhang Q, Hui H, Agrawal K, Karris MAY, Rana TM. An atlas of immune cell exhaustion in HIV-infected individuals revealed by single-cell transcriptomics. Emerg Microbes Infect. 2020 Jan 1;9(1):2333–47.
44. Brinkmann CR, Højen JF, Rasmussen TA, Kjær AS, Olesen R, Denton PW, et al. Treatment of HIV-Infected Individuals with the Histone Deacetylase Inhibitor Panobinostat Results in Increased Numbers of Regulatory T Cells and Limits *Ex Vivo* Lipopolysaccharide-Induced Inflammatory Responses. Fernandez-Sesma A, editor. mSphere [Internet]. 2018 Feb 28 [cited 2021 Oct 20];3(1). Available from: https://journals.asm.org/doi/10.1128/mSphere.00616-17
45. Kazmierski J, Elsner C, Döhner K, Xu S, Ducroux A, Pott F, et al. A Baseline Cellular Antiviral State Is Maintained by cGAS and Its Most Frequent Naturally Occurring Variant rs610913. J Immunol Baltim Md 1950. 2022 Jul 18;ji2100685.
46. Perez VL, Rowe T, Justement JS, Butera ST, June CH, Folks TM. An HIV-1-infected T cell clone defective in IL-2 production and Ca2+ mobilization after CD3 stimulation. J Immunol Baltim Md 1950. 1991 Nov 1;147(9):3145–8.

47. Symons J, Chopra A, Malatinkova E, De Spiegelaere W, Leary S, Cooper D, et al. HIV integration sites in latently infected cell lines: evidence of ongoing replication. Retrovirology. 2017 Dec;14(1):2.
48. Jamaluddin MS, Hu PW, Jan Y, Siwak EB, Rice AP. Short Communication: The Broad-Spectrum Histone Deacetylase Inhibitors Vorinostat and Panobinostat Activate Latent HIV in CD4+ T Cells In Part Through Phosphorylation of the T-Loop of the CDK9 Subunit of P-TEFb. AIDS Res Hum Retroviruses. 2016 Feb 1;32(2):169–73.
49. Harper MS, Guo K, Gibbert K, Lee EJ, Dillon SM, Barrett BS, et al. Interferon-α Subtypes in an Ex Vivo Model of Acute HIV-1 Infection: Expression, Potency and Effector Mechanisms. PLoS Pathog. 2015;11(11):e1005254.
50. Lavender KJ, Gibbert K, Peterson KE, Van Dis E, Francois S, Woods T, et al. Interferon Alpha Subtype-Specific Suppression of HIV-1 Infection In Vivo. J Virol. 2016 Jul 1;90(13):6001–13.
51. Karakoese Z, Schwerdtfeger M, Karsten CB, Esser S, Dittmer U, Sutter K. Distinct Type I Interferon Subtypes Differentially Stimulate T Cell Responses in HIV-1-Infected Individuals. Front Immunol. 2022;13:936918.
52. Guo K, Shen G, Kibbie J, Gonzalez T, Dillon SM, Smith HA, et al. Qualitative Differences Between the IFNα subtypes and IFNβ Influence Chronic Mucosal HIV-1 Pathogenesis. PLoS Pathog. 2020 Oct;16(10):e1008986.
53. Tsai P, Wu G, Baker CE, Thayer WO, Spagnuolo RA, Sanchez R, et al. In vivo analysis of the effect of panobinostat on cell-associated HIV RNA and DNA levels and latent HIV infection. Retrovirology. 2016 Dec;13(1):36.
54. Bartholomeeusen K, Fujinaga K, Xiang Y, Peterlin BM. Histone Deacetylase Inhibitors (HDACis) That Release the Positive Transcription Elongation Factor b (P-TEFb) from Its Inhibitory Complex Also Activate HIV Transcription. J Biol Chem. 2013 May 17;288(20):14400–7.
55. Khoury G, Mota TM, Li S, Tumpach C, Lee MY, Jacobson J, et al. HIV latency reversing agents act through Tat post translational modifications. Retrovirology. 2018 May 11;15(1):36.
56. Kwaa AKR, Talana CAG, Blankson JN. Interferon Alpha Enhances NK Cell Function and the Suppressive Capacity of HIV-Specific CD8+ T Cells. J Virol. 2019 Jan 17;93(3):e01541-18.
57. Edens RE, Dagtas S, Gilbert KM. Histone deacetylase inhibitors induce antigen specific anergy in lymphocytes: a comparative study. Int Immunopharmacol. 2006 Nov;6(11):1673–81.
58. Pace M, Williams J, Kurioka A, Gerry AB, Jakobsen B, Klenerman P, et al. Histone Deacetylase Inhibitors Enhance CD4 T Cell Susceptibility to NK Cell Killing but Reduce NK Cell Function. Swanstrom R, editor. PLOS Pathog. 2016 Aug 16;12(8):e1005782.
59. Triplett TA, Holay N, Kottapalli S, VanDenBerg C, Capasso A. Elucidating the Role of HDACs in T Cell Biology and Comparing Distinct HDAC Inhibitors in Augmenting Responses to Cancer Immunotherapy. J Immunol. 2020 Mai;204(1 Supplement):165.23.
60. Jones RB, O'Connor R, Mueller S, Foley M, Szeto GL, Karel D, et al. Histone Deacetylase Inhibitors Impair the Elimination of HIV-Infected Cells by Cytotoxic T-Lymphocytes. Silvestri G, editor. PLoS Pathog. 2014 Aug 14;10(8):e1004287.
61. Boucau J, Das J, Joshi N, Le Gall S. Latency reversal agents modulate HIV antigen processing and presentation to CD8 T cells. PLoS Pathog. 2020 Mar;16(3):e1008442.
62. Nusinzon I, Horvath CM. Positive and negative regulation of the innate antiviral response and beta interferon gene expression by deacetylation. Mol Cell Biol. 2006 Apr;26(8):3106–13.
63. von Schwedler UK, Stray KM, Garrus JE, Sundquist WI. Functional Surfaces of the Human Immunodeficiency Virus Type 1 Capsid Protein. J Virol. 2003 May;77(9):5439–50.
64. Anokhin B, Spearman P. Viral and Host Factors Regulating HIV-1 Envelope Protein Trafficking and Particle Incorporation. Viruses. 2022 Aug;14(8):1729.
65. von Bredow B, Arias JF, Heyer LN, Gardner MR, Farzan M, Rakasz EG, et al. Envelope

Glycoprotein Internalization Protects Human and Simian Immunodeficiency Virus-Infected Cells from Antibody-Dependent Cell-Mediated Cytotoxicity. J Virol. 2015 Oct;89(20):10648–55.

66. Veillette M, Coutu M, Richard J, Batraville LA, Dagher O, Bernard N, et al. The HIV-1 gp120 CD4-bound conformation is preferentially targeted by antibody-dependent cellular cytotoxicity-mediating antibodies in sera from HIV-1-infected individuals. J Virol. 2015 Jan;89(1):545–51.
67. Veillette M, Désormeaux A, Medjahed H, Gharsallah NE, Coutu M, Baalwa J, et al. Interaction with cellular CD4 exposes HIV-1 envelope epitopes targeted by antibody-dependent cell-mediated cytotoxicity. J Virol. 2014 Mar;88(5):2633–44.
68. Xu HC, Grusdat M, Pandyra AA, Polz R, Huang J, Sharma P, et al. Type I interferon protects antiviral CD8+ T cells from NK cell cytotoxicity. Immunity. 2014 Jun 19;40(6):949–60.
69. Crouse J, Bedenikovic G, Wiesel M, Ibberson M, Xenarios I, Von Laer D, et al. Type I interferons protect T cells against NK cell attack mediated by the activating receptor NCR1. Immunity. 2014 Jun 19;40(6):961–73.
70. Pham TN, Lukhele S, Hajjar F, Routy JP, Cohen ÉA. HIV Nef and Vpu protect HIV-infected CD4+ T cells from antibody-mediated cell lysis through down-modulation of CD4 and BST2. Retrovirology. 2014 Feb 6;11(1):15.
71. Azzoni L, Foulkes AS, Papasavvas E, Mexas AM, Lynn KM, Mounzer K, et al. Pegylated Interferon Alfa-2a Monotherapy Results in Suppression of HIV Type 1 Replication and Decreased Cell-Associated HIV DNA Integration. J Infect Dis. 2013 Jan 15;207(2):213–22.
72. Asmuth DM, Murphy RL, Rosenkranz SL, Lertora JJL, Kottilil S, Cramer Y, et al. Safety, tolerability, and mechanisms of antiretroviral activity of pegylated interferon Alfa-2a in HIV-1-monoinfected participants: a phase II clinical trial. J Infect Dis. 2010 Jun 1;201(11):1686–96.
73. Ogbomo H, Michaelis M, Kreuter J, Doerr HW, Cinatl J. Histone deacetylase inhibitors suppress natural killer cell cytolytic activity. FEBS Lett. 2007 Apr 3;581(7):1317–22.
74. Gruell H, Gunst JD, Cohen YZ, Pahus MH, Malin JJ, Platten M, et al. Effect of 3BNC117 and romidepsin on the HIV-1 reservoir in people taking suppressive antiretroviral therapy (ROADMAP): a randomised, open-label, phase 2A trial. Lancet Microbe. 2022 Mar;3(3):e203–14.
75. Gay CL, James KS, Tuyishime M, Falcinelli SD, Joseph SB, Moeser MJ, et al. Stable Latent HIV Infection and Low-level Viremia Despite Treatment With the Broadly Neutralizing Antibody VRC07-523LS and the Latency Reversal Agent Vorinostat. J Infect Dis. 2022 Mar 2;225(5):856–61.
76. Leth S, Schleimann MH, Nissen SK, Højen JF, Olesen R, Graversen ME, et al. Combined effect of Vacc-4x, recombinant human granulocyte macrophage colony-stimulating factor vaccination, and romidepsin on the HIV-1 reservoir (REDUC): a single-arm, phase 1B/2A trial. Lancet HIV. 2016 Oct;3(10):e463-472.
77. Machnowska P, Meixenberger K, Schmidt D, Jessen H, Hillenbrand H, Gunsenheimer-Bartmeyer B, et al. Prevalence and persistence of transmitted drug resistance mutations in the German HIV-1 Seroconverter Study Cohort. PloS One. 2019;14(1):e0209605.
78. Butler A, Hoffman P, Smibert P, Papalexi E, Satija R. Integrating single-cell transcriptomic data across different conditions, technologies, and species. Nat Biotechnol. 2018 Jun;36(5):411–20.
79. MacLeod MKL, Clambey ET, Kappler JW, Marrack P. CD4 memory T cells: What are they and what can they do? Semin Immunol. 2009 Apr 1;21(2):53–61.
80. Chomont N, El-Far M, Ancuta P, Trautmann L, Procopio FA, Yassine-Diab B, et al. HIV reservoir size and persistence are driven by T cell survival and homeostatic proliferation. Nat Med. 2009 Aug;15(8):893–900.
81. Pušnik J, Eller MA, Tassaneetrithep B, Schultz BT, Eller LA, Nitayaphan S, et al. Expansion of Stem Cell-Like CD4+ Memory T Cells during Acute HIV-1 Infection Is Linked to Rapid Disease Progression. J Virol. 2019 Jun 28;93(14):e00377-19.

82. Kononchik J, Ireland J, Zou Z, Segura J, Holzapfel G, Chastain A, et al. HIV-1 targets L-selectin for adhesion and induces its shedding for viral release. Nat Commun. 2018 Jul 19;9(1):2825.
83. Golubovskaya V, Wu L. Different Subsets of T Cells, Memory, Effector Functions, and CAR-T Immunotherapy. Cancers. 2016 Mar 15;8(3):36.
84. Jain N, Nguyen H, Chambers C, Kang J. Dual function of CTLA-4 in regulatory T cells and conventional T cells to prevent multiorgan autoimmunity. Proc Natl Acad Sci. 2010 Jan 26;107(4):1524–8.
85. Jiang Y, Li Y, Zhu B. T-cell exhaustion in the tumor microenvironment. Cell Death Dis. 2015 Jun;6(6):e1792–e1792.
86. Ramírez F, Ryan DP, Grüning B, Bhardwaj V, Kilpert F, Richter AS, et al. deepTools2: a next generation web server for deep-sequencing data analysis. Nucleic Acids Res. 2016 Jul 8;44(W1):W160-165.
87. Metsalu T, Vilo J. ClustVis: a web tool for visualizing clustering of multivariate data using Principal Component Analysis and heatmap. Nucleic Acids Res. 2015 Jul 1;43(W1):W566-570.
88. Wang J, Duncan D, Shi Z, Zhang B. WEB-based GEne SeT AnaLysis Toolkit (WebGestalt): update 2013. Nucleic Acids Res. 2013 Jul;41(Web Server issue):W77-83.
89. Zhang B, Kirov S, Snoddy J. WebGestalt: an integrated system for exploring gene sets in various biological contexts. Nucleic Acids Res. 2005 Jul 1;33(Web Server issue):W741–8.
90. Mi H, Thomas P. PANTHER Pathway: an ontology-based pathway database coupled with data analysis tools. Methods Mol Biol Clifton NJ. 2009;563:123–40.
91. Garcia-Alonso L, Holland CH, Ibrahim MM, Turei D, Saez-Rodriguez J. Benchmark and integration of resources for the estimation of human transcription factor activities. Genome Res. 2019 Aug;29(8):1363–75.
92. Holland CH, Tanevski J, Perales-Patón J, Gleixner J, Kumar MP, Mereu E, et al. Robustness and applicability of transcription factor and pathway analysis tools on single-cell RNA-seq data. Genome Biol. 2020 Feb 12;21(1):36.
93. Jassal B, Matthews L, Viteri G, Gong C, Lorente P, Fabregat A, et al. The reactome pathway knowledgebase. Nucleic Acids Res. 2020 Jan 8;48(D1):D498–503.
94. Liberzon A, Subramanian A, Pinchback R, Thorvaldsdóttir H, Tamayo P, Mesirov JP. Molecular signatures database (MSigDB) 3.0. Bioinforma Oxf Engl. 2011 Jun 15;27(12):1739–40.
95. Laue M. Electron microscopy of viruses. Methods Cell Biol. 2010;96:1–20.
96. Richard J, Veillette M, Batraville LA, Coutu M, Chapleau JP, Bonsignori M, et al. Flow cytometry-based assay to study HIV-1 gp120 specific antibody-dependent cellular cytotoxicity responses. J Virol Methods. 2014 Nov;208:107–14.
97. Alter G, Malenfant JM, Altfeld M. CD107a as a functional marker for the identification of natural killer cell activity. J Immunol Methods. 2004 Nov;294(1–2):15–22.